NASA CONTRACTOR REPORT

NASA CR-2834

DEVELOPMENT OF A DIGITAL AUTOMATIC CONTROL LAW FOR STEEP GLIDESLOPE CAPTURE AND FLARE

Nesim Halyo

Prepared by
UNIVERSITY OF VIRGINIA
Charlottesville, Va. 22901
for Langley Research Center

NATIONAL AERONAUTICS AND SPACE ADMINISTRATION • WASHINGTON, D. C. • JUNE 1977

1. Report No.	2. Government Accession No.	3. Recipient's Catalog No.
NASA CR-2834		

4. Title and Subtitle	5. Report Date
Development of a Digital Automatic Control Law for Steep Glideslope Capture and Flare	June 1977
	6. Performing Organization Code
7. Author(s)	8. Performing Organization Report No.
Nesim Halyo	
	10. Work Unit No.
9. Performing Organization Name and Address	
University of Virginia Charlottesville, VA 22901	11. Contract or Grant No.
	NAS1-12754, 2
	13. Type of Report and Period Covered
12. Sponsoring Agency Name and Address	Contractor Report
National Aeronautics and Space Administration Washington, DC 20546	14. Sponsoring Agency Code

15. Supplementary Notes

Final Report

Langley Technical Monitor; Richard M. Hueschen

16. Abstract

A longitudinal digital guidance and control law for steep glideslopes using MLS (Microwave Landing System) data is developed for CTOL aircraft using modern estimation and control techniques. The control law covers the final approach phases of glideslope capture, glideslope tracking, flare to touchdown for automatic landings under adverse weather conditions. The control law uses a constant gain Kalman filter to process MLS and body-mounted accelerometer data to form estimates of flight path errors and wind velocities including wind shear. The flight path error estimates and wind estimates are used for feedback in generating control surface commands. Results of a digital simulation of the aircraft dynamics and the guidance and control law are presented for various wind conditions.

17. Key Words (Suggested by Author(s))	18. Distribution Statement
Optimal Control, 4D, Steep Approach, Automatic landing, Flare, Noise Abatement, Kalman Filtering, Approach, Glideslope Capture	Unclassified - Unlimited Subject Category 05

19. Security Classif. (of this report)	20. Security Classif. (of this page)	21. No. of Pages	22. Price*
Unclassified	Unclassified	67	$4.50

*For sale by the National Technical Information Service, Springfield, Virginia 22161

TABLE OF CONTENTS

LIST OF FIGURES

LIST OF TABLES

SECTION I
INTRODUCTION

This study considers the development of a digital 4D automatic control law to capture a steep glideslope, flare and land a CTOL aircraft under low visibility and adverse wind conditions using the Microwave Landing System (MLS) under development by the FAA [1], [2], The study of curved 4D flight paths leading to a steep final approach under low visibility (up to CAT III C) and adverse wind conditions is part of the Terminal Configured Vehicle (TCV) program sponsored jointly by NASA and FAA [3]. The goals of the TCV program include the reduction of aircraft noise in airport communities, the reduction of the adverse effects of weather conditions on the efficiency of aircraft operations in air terminals, the reduction of fuel consumption, and the efficient use of airspace in congested terminal areas through the use of the Microwave Landing System and the development of technology.

The major effect of the use of steep glideslopes in the final landing is in the area of noise reduction. In comparison to the currently used 2.5° to 3° ILS glideslopes, a 5° to 6° glideslope reduces the noise level on the ground due to differences in the altitude profiles and thrust levels. At equal distances from the runway, the altitude of an aircraft on a 6° glideslope is almost twice the altitude of an aircraft on a 3° glideslope. Thus, if both aircraft were to generate the same amount of noise, the noise level perceived on the ground would be reduced due to the 2:1 ratio in the altitudes. A further reduction in noise is due to the fact that the aircraft following a 6° glideslope requires a lower thrust setting than the one following a 3° glideslope. For a Boeing 737 the reduction in the thrust levels is of the order of 2:1. Thus, for a steep glideslope less engine noise is generated.

The reduction in thrust level associated with steep glideslopes also reduces the fuel consumption during the final approach. The ability to fly glideslope of varying angles may also provide a method to avoid the vortex generated by large aircraft, by allowing smaller aircraft to fly different glideslopes to reduce the likelihood of such

encounters. In general, the ability to fly steep glideslopes provides a versatility that can be useful in efficient use of airspace in the terminal area.

The guidance information necessary to fly steep glideslopes under low visibility conditions is provided by the Microwave Landing System (MLS). The MLS is a ground-based guidance system providing position information to aircraft which are inside its volumetric coverage at discrete intervals of time. Thus, aircraft have accurate position information to fly glideslopes of varying angles, and follow curved 4D paths to landing within the MLS coverage under low visibility conditions. The MLS consists of a DME providing range information, an azimuth antenna co-located with the DME providing the aircraft's azimuth angle relative to the runway, and an elevation antenna located at the glidepath intercept point (GPIP) but offset to the side of the runway providing the aircraft with its elevation angle relative to the local horizon. The azimuth antenna provides coverage up to $\pm$ 60°, the elevation coverage is up to 20°. A second elevation antenna located further down the runway is also under consideration for flare guidance. Thus, the MLS provides position information with a high accuracy in a volumetric coverage, with low sensitivity to adverse weather conditions.

In this study, a longitudinal guidance and control law using MLS data and body-mounted accelerometers is developed for the final approach phases from glideslope capture to touchdown.

In Section II, the aircraft equations of motion and the wind model are described. A mathematical model describing the perturbations of the aircraft from a 6° glideslope is obtained for the longitudinal axis; the first order effects of lags in the effects of winds on the motion of the aircraft and thrust build-up are included in this model. Using the Dryden spectra, a dynamic model of gusts is developed; these steady winds and wind shear models are combined to obtain a total wind model. These mathematical models are used in simulating the aircraft's motion under various wind conditions. In Section III, the desired flight path is described and formulated in a form suitable to the

development of the digital control law. In Section IV, the development of the digital control law is described. The control law consists of a filter estimating error parameters and wind velocities which are used as feedback to compute control commands. Section V describes the results obtained from a digital simulation of the aircraft using the guidance and control law developed.

II. AIRCRAFT DYNAMICS AND WIND MODELING

The aircraft equations of motion are used in simulating aircraft's flight and in the development and analysis of the control law. Similarly, the wind model is used in generating various turbulence levels and the development of the filtering equations. To obtain a suitable mathematical model of the aircraft dynamics and the effects of various wind conditions on the motion of the aircraft, the general equations of motion can be linearized about a steep glideslope at an airspeed of 120 knots with fully extended flaps and landing gear down. Thus, a linear mathematical model describing the perturbations of the aircraft motion from the steady flight condition of glideslope tracking is obtained. This model can then be used to simulate the aircraft's motion and for analysis. In the general perturbation equations (e.g. [4], pp. 2.33), the aircraft's lateral and vertical motions are coupled. This coupling is mainly due to a non-zero roll angle. As the phases of flight considered are glideslope capture, glideslope tracking and flare (as shown in Figure 1), the roll angle is small, and can be expressed as a perturbation from a steady value of zero. In this case, the lateral and vertical motions are decoupled. Thus, the longitudinal equations of motion can be used to simulate the aircraft's motion in the vertical plane. The longitudinal equations can then be expressed in the stability axes as

$$m\dot{u} = - mg \cos\gamma_o \, \theta + f_{a_x} + f_{T_x} \tag{1a}$$

$$m(\dot{w} - U_o q) = - mg \sin \gamma_o \, \theta + f_{A_z} + f_{T_z} \tag{1b}$$

$$I_{yy} \dot{q} = m_A + m_T \tag{1c}$$

where

U_o - steady inertial speed in the x_s direction

γ_o - glideslope angle

θ - perturbation in pitch angle

q - pitch rate

f_{A_x} - perturbation in net aerodynamic force along the x_s direction

f_{A_z} - perturbation in net aerodynamic force along the z_s direction

f_{T_x} - perturbation in thrust along the x_s direction

f_{T_z} - perturbation in thrust along the z_x direction

m_A - perturbation in pitching moment due to aerodynamic forces

m_T - perturbation in pitching moment due to thrust

I_{yy} - moment of inertia about the y_s axis

m - aircraft mass

u - perturbation in inertial speed along the x_s direction

w - inertial speed along the z_s direction

Mainly, three sets of coordinate axes are used in this study: the earth fixed axes, the body axes, and the stability axes. The earth-fixed ccordinate frame (x_e, y_e, z_e) has its origin fixed at the glidepath intercept point (GPIP) on the runway. The x_e axis is along the runway centerline, the direction in which the aircraft lands being chosen positive velocity along x_e. The z_e axis is the local vertical positive downwards; y_e is perpendicular to both x_e and z_e, with its positive end directed so as to make the coordinate frame right-handed. The earth is assumed to be stationary with respect to inertial space; so that the earth-fixed axes form an inertial frame.

The body axes (x_b, y_b, z_b) and the stability axes (x_s, y_s, z_s) are fixed to the body of the aircraft; i.e. they are body-fixed axes. The origin of both axes is fixed at the aircraft center of mass. The x_b axis

is along the fuselage reference line of the aircraft, positive towards the nose, the y_b axis is positive towards the tip of the right wing; the z_b axis is perpendicular to both x_b and y_b and is positive downwards (when the aircraft pitch angle is zero). The stability axes (x_s, y_s, z_s) are obtained from the body axes by a rotation of α_o, the steady state angle of attack, about the y_b axis. Three sets of coordinate frames are shown in Figure 2.

In equation (1), the term f_{A_x} represents the total algebraic change in the value of the aerodynamic force along the x_s axis due to changes from steady state values in the values of the aerodynamic and control variables; the terms f_{A_z}, f_{T_z}, f_{A_x}, m_A and m_T are defined similarly as the changes in the appropriate forces or moments from their steady values on the glideslope. These terms can be expressed in terms of the aircraft stability derivatives, the moments of inertia and the perturbations in the aerodynamic and control variables. Substituting these expressions for the force and moments into equation (1) the aircraft equations of motion can be expressed as given below.

$$m\dot{u} = - mg \cos\gamma_o \theta + \bar{q}_o S\{(-C_{D_{\underline{u}'}} + 2C_{D_o} + C_{T_{x\underline{u}'}} + 2C_{T_{xo}}) \underline{u}'$$

$$+ (C_{Lo} - C_{D\underline{\alpha}}) \underline{\alpha} - C_{D\delta_e} \delta e - C_{D\delta S} \delta s + C_{TX\delta T} \delta T\} \qquad (2a)$$

$$m(\dot{w} - u_o q) = - mg \sin\gamma_o \theta + \bar{q}_o S \{-(C_{L\underline{u}'} + 2C_{Lo}) \underline{u}'$$

$$- (C_{L\alpha} + C_{Do}) \underline{\alpha} - C_{L\underline{\dot{\alpha}}} \underline{\dot{\alpha}} - C_{L\underline{q}} \underline{q}\} \qquad (2b)$$

$$I_{yy} \dot{q} = \bar{q}_o S\bar{c} \{(C_{M\underline{u}'} + 2C_{Mo}) \underline{u}' + (C_{M\underline{\alpha}} + C_{MT\underline{\alpha}}) \underline{\alpha} + C_{M\underline{\dot{\alpha}}} \underline{\dot{\alpha}}$$

$$+ C_{M\underline{q}} \underline{q} + C_{M\delta e} \delta e + C_{M\delta s} \delta_S + C_{M\delta T} \delta T\}. \qquad (2c)$$

where

$$\underline{u}' = \frac{u + u_w}{U_o} \qquad (3a)$$

$$\underline{\alpha} = \alpha + \alpha_w \quad , \tag{3b}$$

$$\underline{q} = q + q_w \quad , \tag{3c}$$

u_w, α_w, and q_w are the components due to wind, $\bar{q}_o$ is the steady value of the dynamic pressure, S is the effective wing area, δe, δs and δT are the perturbations of elevator, stabilizer and thrust, respectively.

Equation (2) describes the linear and angular velocities of the aircraft. The position of the aircraft can be obtained by integrating the inertial velocity components over time. Thus, the 4D error in position (i.e., the actual position relative to the desired position at a given time) can be linearized and expressed in the following form:

$$\frac{\dot{x} - \dot{x}_o}{U_o} = - \sin\gamma_o \, \theta + \cos\gamma_o \, u' + \sin\gamma_o \, \alpha \tag{4a}$$

$$\frac{\dot{z} - \dot{z}_o}{U_o} = - \cos\gamma_o \, \theta - \sin\gamma_o \, u' + \cos\gamma_o \, x \tag{4b}$$

where $x_o(t)$ and $z_o(t)$ are the x_e and z_e coordinates of the desired aircraft position on the glideslope. The desired glideslope position in this case was taken to be the position of the aircraft going down a 6° glideslope at 120 knots inertial speed.

The effects of the servo responses of the actuators were modeled by first and second order systems. Thus, the thrust and stabilizer models are

$$\dot{\delta T} = - .5 \, \delta T + .298 \, \delta th, \quad , \tag{5a}$$

$$\dot{\delta th} = u_3 \quad , \tag{5b}$$

$$\dot{\delta s} = u_2 \quad ; \tag{5c}$$

where δT is the thrust perturbation in thousands of pounds, δth is the throttle position perturbation in degrees and δs is the stabilizer position perturbation in radians. As the lags in elevator action are small, the elevator time constants were neglected. The aircraft equations of motion (2), the position equations (4) and the actuator equations (5) can be combined and after some manipulation expressed in state variable form as shown in equation (6).

$$x' = (\theta\ u'\ \alpha\ q\ \frac{x - x_o}{Uo}\ \ \frac{z - z_o}{Uo}\ \delta T\ \delta th\ \delta s), \tag{6a}$$

$$u' = (\delta e\ \dot{\delta s}\ \dot{\delta th}), \quad w' = (u'_w\ \alpha_w\ q_w) \tag{6b}$$

$$\dot{x} = Ax + Bu + Dw\ , \tag{6c}$$

where A, B and D are matrices of appropriate size, corresponding to the coefficients in equations (2), (4) and (5). These matrices are given in terms of the aircraft stability derivatives in the Appendix. For a more detailed derivation of the models given here see [5]. Thus, the aircraft equations of motion and the 4D error equations for sink rate and ground speed have been modeled in state variable form as shown in equation (6).

The wind model contains the components of steady wind velocities, turbulence and shear winds in the longitudinal axis. The turbulence model uses the Dryden spectra [6] for the various components varying with altitude. The turbulence model has three components: u'_g in the x_b direction, α_g in the z_b direction and q_g which models the effects of turbulence on the pitch rate of the aircraft. These components are modeled using the following spectra.

$$S_u(\Omega) = \frac{2\ \sigma_u^2\ L_u}{1 + (L_u \Omega)^2}\ , \tag{7a}$$

$$S_\alpha(\Omega) = \frac{\sigma_w^2\ L_w}{Va^2}\ \frac{1 + 3(L_w\ \Omega)^2}{[1 + (L_w\ \Omega)^2]^2}\ , \tag{7b}$$

$$S_q(\Omega) = \frac{\Omega^2 \, Va^2}{1 + (\frac{4b}{\pi}\Omega)^2} S_\alpha(\Omega) \quad , \tag{7c}$$

where b is the wing span, L_u and L_w are the scales of turbulence, Va is the airspeed, and Ω is the spatial frequency related to the temporal frequency w by

$$\Omega = w/Va \; . \tag{8}$$

The u'_g component is independent of α_g and q_g, however, α_g and q_g are correlated with their cross spectral density being

$$S_{q\alpha}(w) = \frac{jw}{1 + j\frac{4b}{\pi Va} w} S_\alpha(w) \; . \tag{9}$$

The above spectra can be factored using spectral factorization methods to obtain a linear system driven by white noise which generates an output having the above spectral characteristics [7], [8]. Thus, the following transfer functions are obtained to generate u'_g, α_g and q_g.

$$G_u(s) = \frac{1}{1 + \frac{L_u}{Va} s} \quad , \tag{10a}$$

$$G_\alpha(s) = \frac{1 + \sqrt{3}\frac{L_w}{Va} s}{1 + 2\frac{L_w}{Va} s + (\frac{L_w}{Va})^2 s^2} \quad , \tag{10b}$$

$$G_q(s) = \frac{s}{1 + \frac{4b}{\pi Va} s} \quad , \tag{10c}$$

where α_g is the input to the system $G_q(s)$ to obtain q_g with the specified spectrum and cross-spectral density. Figure 3 shows a block diagram of the system generating the turbulence components.

The steady and shear wind in the longitudinal direction was modeled by

$$\dot{u}'_s = u'_{sg} \quad , \quad \dot{u}'_{sh} = W_3 \quad , \tag{11a}$$

$$\dot{\alpha}_s = W_4 \quad . \tag{11b}$$

Thus, to simulate a specified shear profile for $\dot{u}'_s$, with appropriate initial conditions; e.g., to obtain a linear profile u'_s changing at a rate of u'_{sho}, the initial condition for u'_{sh} is set to u'_{sho} and W_3 is set equal to zero; alternately, an impulse in W_3 will also achieve the same profile.

The transfer functions obtained for the wind model can equivalently be expressed as differential equations in state variable form as shown in (12); the matrices A_W, B_W and C_W are given in the Appendix.

$$\dot{W} = A_W W + B_W \zeta \ , \ w = C_W W \quad , \tag{12}$$

where w is given by equation (6b).

III. FLIGHT PATH MODELING

In this section, the desired flight path for the aircraft will be modeled as a vector differential equation. In Section IV, the solution to the optimal control problem of following a flight path specified in state variable form will be presented. The flight path of interest here consists of a steep glideslope and flare. First consider the flight path describing the glideslope, which will be called the reference flight path as the equations of motion obtained in the preceeding section are linearized about this flight condition. Let Z_r be a vector where Z_{r_1} represents the pitch angle, Z_{r_2} the speed in the x_s direction, Z_{r_3} the speed in the z_s direction, Z_{r_4} the pitch rate, Z_{r_5} and Z_{r_6} the x_e and z_e components of the aircraft position respectively, Z_{r_7} the thrust force, Z_{r_8} the throttle position, and Z_{r_9} the stabilizer position. Then, the reference glideslope flight path can be described by the following set of differential equations.

$$\dot{Z}_{r_1} = Z_{r_4}$$

$$\dot{Z}_{r_2} = 0$$

$$\dot{Z}_{r_3} = 0$$

$$\dot{Z}_{r_4} = 0 \qquad (13)$$

$$\dot{Z}_{r_5} = -U_o \sin\gamma_o \, Z_{r_1} + \cos\gamma_o \, Z_{r_2} + \sin\gamma_o \, Z_{r_3} + \zeta_{r_5}$$

$$\dot{Z}_{r_6} = -U_o \cos\gamma_o \, Z_{r_1} - \sin\gamma_o \, Z_{r_2} + \cos\gamma_o \, Z_{r_3} + \zeta_{r_6}$$

$$\dot{Z}_{r_7} = 0$$

$$\dot{Z}_{r_8} = 0$$

$$\dot{Z}_{r_9} = 0$$

$$\text{where } \zeta_{r_5} = U_o \, \theta_o \sin\gamma_o \, , \; \zeta_{r_6} = U_o \, \theta_o \cos\gamma_o \qquad (14)$$

θ_o is the steady state pitch angle, and the initial conditions are given by

$$Z_{r_1} = \theta_o,\ Z_{r_2} = U_o,\ Z_{r_3} = Z_{r_4} = 0\ ,\ Z_{r_5} = x_o \tag{15a}$$

$$Z_{r_6} = -\ h_o,\ Z_{r_7} = T_o,\ Z_{r_8} = T_{h_o}\ ,\ Z_{r_9} = s_o\ . \tag{15b}$$

Thus, the glidepath condition can be described by the equation

$$\dot{Z}_r = \underline{A}\ Z_r + \underline{\zeta_r} \tag{16}$$

where the matrix $\underline{A}$ corresponds to the coefficients in equation (13). The desired flight path can also be described by an equation similar to equation (16).

$$\begin{aligned}
\dot{Z}_1 &= Z_4 + \underline{\zeta_1} \\
\dot{Z}_2 &= \underline{\zeta_2} \\
\dot{Z}_3 &= \underline{\zeta_3} \\
\dot{Z}_4 &= \underline{\zeta_4} \\
\dot{Z}_5 &= -\ U_o \sin\gamma_o\ Z_1 + \cos\gamma_o\ Z_2 + \sin\gamma_o\ Z_3 + \underline{\zeta_5} \\
\dot{Z}_6 &= -\ U_o \cos\gamma_o\ Z_1 - \sin\gamma_o\ Z_2 + \cos\gamma_o\ Z_3 + \underline{\zeta_6} \\
\dot{Z}_7 &= \underline{\zeta_7} \\
\dot{Z}_8 &= \underline{\zeta_8} \\
\dot{Z}_9 &= \underline{\zeta_9}
\end{aligned} \tag{17}$$

To define the desired flight path completely, $\underline{\zeta}_i$ must be specified. Thus, let x_d and z_d be the desired position coordinates in the earth-fixed coordinate frame, then setting

$$\begin{aligned}
\underline{\zeta}_2 &= \ddot{x}_d \cos(Z_1 - \alpha_o) - \ddot{z}_d \sin(Z_1 - \alpha_o) - Z_3 Z_4 \\
\underline{\zeta}_3 &= \ddot{x}_d \sin(Z_1 - \alpha_o) + \ddot{z}_d \cos(Z_1 - \alpha_o) + Z_2 Z_4 \\
\underline{\zeta}_5 &\quad \dot{x}_d [1 - \cos(Z_1 - Z_{r_1})] + \dot{z}_d \sin(Z_1 - Z_{r_1}) + U_o \sin\gamma_o Z_1 \\
\underline{\zeta}_6 &= -\dot{x}_d \sin(Z_1 - Z_{r_1}) + \dot{z}_d [1 - \cos(Z_1 - Z_{r_1})] + U_o \cos\gamma_o Z_1
\end{aligned} \tag{18}$$

would result in

$$Z_5 = x_d, \quad Z_6 = z_d \quad ,$$

while Z_2 and Z_3 would correspond to the desired velocity components in the stability axes. Note that $\underline{\zeta}_1$, $\underline{\zeta}_4$, $\underline{\zeta}_7$, $\underline{\zeta}_8$ and $\underline{\zeta}_9$ should be chosen appropriately, so as to aid in the performance of following the desired flight path; these are specified with due consideration to the aerodynamic characteristics of the aircraft. Thus, the desired flight path can also be expressed in the form of equation (16).

$$\dot{Z} = \underline{A}Z + \underline{\zeta} \tag{19}$$

Subtracting the reference flight path Z_r from the desired flight path Z, we obtain the deviations of the desired flight path from the reference glidepath. Further, normalizing the velocity components $Z_2 - Z_{r_2}$, $Z_3 - Z_{r_3}$, and the position components $Z_5 - Z_{r_5}$, $Z_6 - Z_{r_6}$ by the nominal speed U_o of the aircraft, we form a normalized vector, say z, describing the desired flight path relative to the reference flight path. Using (13) - (19), z can be expressed as

$$\dot{z} = A_z z + \zeta \quad , \tag{20}$$

where

$$A_z = \begin{bmatrix} 0 & 0 & 0 & 1 & 0 & 0 & 0 & 0 & 0 \\ 0 & 0 & 0 & 0 & 0 & 0 & 0 & 0 & 0 \\ 0 & 0 & 0 & 0 & 0 & 0 & 0 & 0 & 0 \\ 0 & 0 & 0 & 0 & 0 & 0 & 0 & 0 & 0 \\ -\sin\gamma_o & \cos\gamma_o & \sin\gamma_o & 0 & 0 & 0 & 0 & 0 & 0 \\ -\cos\gamma_o & -\sin\gamma_o & \cos\gamma_o & 0 & 0 & 0 & 0 & 0 & 0 \\ 0 & 0 & 0 & 0 & 0 & 0 & 0 & 0 & 0 \\ 0 & 0 & 0 & 0 & 0 & 0 & 0 & 0 & 0 \\ 0 & 0 & 0 & 0 & 0 & 0 & 0 & 0 & 0 \end{bmatrix} \tag{21}$$

$$\zeta_2 = \frac{\ddot{x}_d}{U_o} \cos(\gamma_o + z_1) - \frac{\ddot{z}_d}{U_o} \sin(\gamma_o + z_1) - z_3 z_4$$

$$\zeta_3 = \frac{\ddot{x}_d}{U_o} \sin(\gamma_o + z_1) + \frac{\ddot{z}_d}{U_o} \cos(\gamma_o + z_1) + (1 + z_2)\, z_4 \tag{22}$$

$$\zeta_5 = \frac{\dot{x}_d}{U_o} (1 - \cos z_1) + \frac{\dot{z}_d}{U_o} \sin z_1 + \sin\gamma_o\, z_1$$

$$\zeta_6 = \frac{\dot{x}_d}{U_o} \sin z_1 + \frac{\dot{z}_d}{U_o} (1 - \cos z_1) + \cos\gamma_o\, z_1$$

Since the aircraft dynamics equations (6) are expressed as deviations from the reference glidepath, z describes the desired trajectory values for the vector x in equation (6). Thus, in the following we shall call z the desired flight path. Now, to define the desired flight path ż, it is necessary to specify ζ, hence $\dot{x}_d$, $\ddot{x}_d$, $\dot{z}_d$ and z_d.

When the aircraft is following the glideslope, the desired deviation from the reference flight path is zero. Thus, an initial condition of zero for all the components of z and setting ζ equal to zero in equation (20) generates the glideslope as the desired flight path. During flare, the desired flight path differs from the glideslope;

During this portion of the flight z will thus be different than zero. The flare flight path was determined by a constant deceleration in the vertical and longitudinal directions. Thus, the desired flare path starts with a specified sink rate $\dot{z}_{dg}$ (i.e. the glideslope sink rate), and a specified ground speed $\dot{x}_{dg}$, and using constant decelerations $\ddot{z}_d$ and $\ddot{x}_d$ decelerates to specified speeds $\dot{z}_{df}$ and $\dot{X}_{df}$ at a specified point z_{df} and X_{df} and then maintains its speed till touchdown. With the above constraints, it is possible to determine the unspecified variables to obtain the following relations

$$\ddot{z}_d = \frac{\dot{z}_{df} - \dot{z}_{dg}}{\dot{x}_{dg} - \dot{x}_{df}} \ddot{x}_d \tag{23a}$$

$$\ddot{x}_d = \frac{1}{2} \frac{\dot{x}_{dg}^2 - \dot{x}_{df}^2}{x_{df} - x_{dg}} \tag{23b}$$

$$x_{df} = x_{td} + \frac{z_{df}}{\dot{z}_{df}} \dot{x}_{df} \tag{23c}$$

$$x_{dg} = \frac{z_{dg}}{-\tan\gamma_o} \quad , \tag{23d}$$

$$z_{dg} = \frac{z_{df} - \dfrac{\dot{z}_{dg} + \dot{z}_{df}}{\dot{x}_{dg} + \dot{x}_{df}}}{1 + \dfrac{\dot{z}_{dg} + \dot{z}_{df}}{\dot{x}_{dg} + \dot{x}_{df}} \dfrac{1}{\tan\gamma_o}} \quad . \tag{23e}$$

Thus, specifying the desired velocity at the start of flare (i.e. $\dot{x}_{dg}$, $\dot{z}_{dg}$), the desired velocity at the end of flare (i.e. $-\dot{z}_{df}$), and the desired touchdown point (i.e. x_{td}) the remaining variables can be determined using equation (23). The instaneous velocity components during flare can be computed using

$$\dot{x}_d(t) = \dot{x}_{dg} - \ddot{x}_d(t - t_g) \quad , t \geq t_g \tag{24a}$$

$$\dot{z}_d(t) = \dot{z}_{dg} + \ddot{z}_d(t = t_g) \quad , t \geq t_g \tag{24b}$$

where t_g is the time at which flare is initiated.

Using equation (23) and (24), $\dot{x}_d$, $\dot{z}_d$, $\ddot{x}_d$ and $\ddot{z}_d$ can be computed, then these values are used to compute instantaneous values for ζ in equation (22) which generates the desired flight path z given by equation (20). The desired pitch during flare was generated by a constant pitch rate until the desired pitch angle reached a specified value θ_f. The thrust, throttle and stabilizer positions were set to their values on the glideslope; however, the throttle and stabilizer components were not weighed in the cost function, thus allowing deviations from their desired values without any associated penalty. This allowed the use of throttle and stabilizer to be determined by the dynamics of the aircraft required to follow the desired flight path.

Thus, the approach taken here allows the desired flight path to be specified in a simple manner by choosing the velocity and acceleration associated with a given path. The desired flight path was described by a set of differential equations in state variable form as given in equation (20). Thus, the values generated by equation (20) for the state vector z are the values that the aircraft dynamics state vector should ideally have. Hence, the difference between the actual aircraft state and the desired state, i.e. x - z, describes the error or the deviations from the desired flight path, the goal of controlling the aircraft being to keep these deviations as small as possible.

IV. DEVELOPMENT OF FILTER AND CONTROL LAW

In the previous sections, the aircraft's longitudinal motion was modeled by equation (6) including the response to control surface and thrust changes under various wind conditions. The wind conditions were modeled by steady winds, random gusts and shear in equation (12). In the last section, the desired flight path during glideslope tracking and flare was expressed by equation (20). In this section, these models are combined to develop a control law to follow the desired flight path; i.e. to capture a steep glideslope, follow the glideslope until flare altitude and follow the flare path to touchdown under various wind conditions including gusts and shear winds, utilizing MLS data and body-mounted accelerometer data.

The control law is developed by imbedding the problem of following a specified flight path into a quadratic regulator with disturbance problem [9], [10]. As the separation principle holds for this problem, the control law consists of a filter in cascade with a feedback control law.

A. Development of the Control Law

The desired flight path consists of capturing the glideslope, following the glideslope till flare altitude, then following the flare path to touchdown. This flight path is described by equations (20) (23) and (24) in state variable form. The difference between x and z is the error in the actual flight path. Combining equation (6) and (20),

$$\dot{x} - \dot{z} = Ax + Bu + D\dot{w} - A_z z - \zeta \; ; \tag{25}$$

rearranging terms,

$$\dot{e} = Ae + Bu + Dw + (A - A_z)\, z - \zeta \; , \tag{26a}$$

$$e = x - z \quad . \tag{26b}$$

The last three terms in the right-hand-side of equation (26a) can be combined as follows.

$$w'_d = (w' \; z' \; \zeta') \quad , \tag{27a}$$

$$D_d = (D \quad (A - A_z) \quad -I) \tag{27b}$$

$$\dot{e} = Ae + Bu + D_d w_d \quad . \tag{27c}$$

From equation (27c), we can see that the problem of following a desired trajectory can also be interpreted as a regulator problem with disturbances by considering the error in the actual trajectory; i.e., the difference between the actual and desired trajectories. To use the results for this problem, the disturbances must be expressed in state variable form and the cost function expressed in terms of the error, e. Thus, combining the wind model with the model for the desired flight path, we get

$$\dot{d} = A_d \, d + n \quad , \tag{28a}$$

$$w_d = C_d \, d \quad , \tag{28b}$$

where

$$d' = (w' \; z' \; \zeta') \quad , \tag{29a}$$

$$A_d = \begin{bmatrix} A_w & 0 & 0 \\ 0 & A_z & 0 \\ 0 & 0 & 0 \end{bmatrix} \quad , \tag{29b}$$

$$C_d = \begin{bmatrix} C_w & 0 & 0 \\ 0 & I & 0 \\ 0 & 0 & I \end{bmatrix} \quad ; \tag{29c}$$

$$n = \begin{bmatrix} B_w & \xi \\ 0 & \\ \xi_1 & \end{bmatrix} \quad . \tag{29d}$$

Note that if we let ξ_1 be a gaussian white noise process, then ζ would be a Brownian motion process. Thus, $z(t)$ would be statistically described by a spectrum shaped by equation (20). Using this approach, the desired flight path is assumed to be a sample function (or a realization) of a random process $z(t)$ with a specified power spectral density. The control law would be independent of the specific sample function, and be applicable to a class of flight paths. An important advantage of this method over the usual quadratic tracking problem ([11] pp. 219-227) is the fact that the desired flight can be specified on line, i.e. the desired flight path can be altered without having to make any modifications to the control law. A second advantage of this method is that a set of constant gains can be obtained by solving for the steady state solution, which would not be possible in a finite time problem.

Since the objective is to follow the desired flight path z, minimizing a cost function which is quadratic in the error x - z is appropriate; hence,

$$J = \frac{1}{2} E \int_0^{t_f} [(x - z)' Q (x - z) + u' R u] dt \quad . \tag{30}$$

Substituting equation (26b) for the error term, we obtain

$$J = \frac{1}{2} E \int_0^{t_f} [e' Q e + u' R u] dt \quad , \tag{31}$$

where E is the statistical expectation operator. Now, since a digital control law is desired, the control variables can vary only at distinct invertals of time say at sampling intervals of T seconds, thus,

$$u(t) = u_k, \quad kT \leq t < kT + T \quad . \tag{32}$$

Thus, equations (27c), (28), (31) and (32) together with linear measurements pose a quadratic regulator problem with random disturbances which has been treated in [5], [9]. With equation (32), equation (27c) can be viewed as a sampled-data system and can be expressed in discrete form [5]

$$e_{k+1} = \phi\, e_k + \Gamma\, u_k + \Gamma_d\, d_k + \eta_k \quad , \tag{33}$$

where ϕ is the transition matrix corresponding to A, Γ is the system control gain, Γ_d is the system disturbance gain and η_k is a white noise sequence. The disturbance equation (28) can also be expressed in discrete form

$$d_{k+1} = \phi_d\, d_k + \eta_k \quad , \tag{34}$$

Where ϕ_d is the transition matrix corresponding to A_d, and η_k is a white noise sequence. The cost function J can also be equivalently expressed in discrete form using equations (27) and (28), [5], to obtain

$$J_1 = \frac{1}{2} E \sum_{k=0}^{N} e'_k \hat{Q} e_k + u'_k \hat{R}\, u_k + 2\,(e'_k\, \hat{N} d_k + e'_k \hat{M} u_k + d'_k \hat{S}] \tag{35}$$

$$\hat{Q} = \int_0^T \phi'(s)\, Q\, \phi(s)\, ds \quad , \tag{36a}$$

$$\hat{R} = \int_0^T \Gamma'(s)\, Q\, \Gamma(s)\, ds + RT \quad , \tag{36b}$$

$$\hat{M} = \int_0^T \phi'(s)\, Q\, \Gamma(s)\, ds \quad , \tag{36c}$$

$$\hat{N} = \int_0^T \phi'(s)\, Q\, \Gamma_d(s)\, ds \quad , \tag{36d}$$

$$\hat{S} = \int_0^T \Gamma'_d(s)\, Q\, \Gamma(s)\, ds \quad . \tag{36e}$$

Note that the continuous and discrete cost functions J and J_1 differ by a constant which does not depend on the control u_k; hence for minimization purposes the two cost functions are equivalent, i.e., the same control u_k minimizes both J and J_1. Thus, the continuous optimal control problem can be reduced to a discrete one; i.e. minimize J_1 subject to the constraints of equations (33) and (34) while the control u_k may only use past measurements. The solution to the continuous problem posed by equations (27c), (28), (31) and (32) as well as the discrete problem posed by equations (33), (34) and (35) is given by the following control law [5].

$$u_k = - H_{1_k} \hat{e}_k - H_{2_k} \hat{d}_k \quad , \tag{37}$$

Where $\hat{e}_k$ and $\hat{d}_k$ are the least mean-square estimates of e_k and d_k given past measurements respectively, and the gains H_{1_k} and H_{2_k} are defined by the equations

$$H_{1_k} = \hat{R}_k^{-1} G_{1_k} \quad , \quad H_{2_k} = \hat{R}_2^{-1} G_{2_k} \quad , \tag{38a}$$

$$G_{1_k} = \Gamma' P_{1_k} \phi + \hat{M} \quad , \quad G_{2_k} = \Gamma' D_k + S \quad , \tag{38b}$$

$$D_k = P_{1_k} \Gamma d + P_{2_k} \phi_d \quad , \quad \hat{R}_k = \hat{R} + \Gamma' P_{1_k} \Gamma \quad , \tag{38c}$$

while P_{1_k} and P_{2_k} are given by the nonlinear difference equations:

$$P_{1_{k-1}} = \phi' P_{1_k} \phi - G_{1_k}' \hat{R}_k^{-1} G_{1_k} + \hat{Q} \quad , \quad P_{1_N} = \hat{Q} \quad , \tag{39a}$$

$$P_{2_{k-1}} = [\phi - \Gamma \hat{R}_k^{-1} G_{1_k}]' D_k + \hat{N} \quad , \quad P_{2_N} = \hat{N} \quad . \tag{39b}$$

For the finite time problem where t_f and N are finite, the control gains vary with time; however, under very loose restrictions [5], the gains converge to constant values. These constant gains are used in the control system. It should also be noted that the steady state gains

result in a stable closed loop system. To see the effect of the various components, we can write the control as

$$u_k = - [H_e \hat{e}_k + H_w \hat{W}_k + H_z z_k + H_\zeta \zeta_k] \quad . \tag{40}$$

From equation (40), we see that the control law uses the estimate of current flight path error $\hat{e}_k$ to reduce this error to zero; it further uses wind estimates $\hat{W}_k$ to prevent expected disturbances due to winds including shear winds; the last two terms provide lead control to follow the desired flight path. Note that z_k contains velocity terms as well as position. While ζ_k contains acceleration information. Thus, the control law consists of a filter which receives measurements obtained by the MLS and on-board sensors followed by the feedback term given in equation (40). A functional block diagram of the system is shown in Figure 4.

B. Development of Filter Equations

The measurements of aircraft position are obtained from the Microwave Landing System (MLS) [2], which provides azimuth, elevation and range to the aircraft at discrete intervals of time; the other aircraft variables measured by on-board sensors include pitch, pitch rate, barometric altitude, barometric sink rate, calibrated airspeed, and body mounted accelerometer data. In terms of the aircraft variables defined so far in this study, the measurements were expressed as follows.

$$Y_1 = \Theta_o + x_1 + V_1 \tag{41a}$$

$$Y_2 = x_4 + V_2 \tag{41b}$$

$$Y_3 = [(U_o x_5 + x_o - x_a)^2 + (U_o x_6 + z_o - z_a)^2]^{1/2} + V_3 \tag{41c}$$

$$Y_4 = \tan^{-1} \left(\frac{U_o x_6 + z_o - z_e}{U_o x_5 + z_o}\right) \tag{41d}$$

$$Y_5 = -(U_o x_6 + z_o + V_5) \tag{41e}$$

$$Y_6 = -(U_o \dot{x}_6 + \dot{z}_o) V_6 \tag{41f}$$

$$Y_7 = U_o \left[\dot{x}_2 \tan x_3 + \frac{1 + x_2}{\cos^2 x_3} \dot{x}_3 - x_4 (1 + x_2 + \cos x_1 - \cos x_3)\right] + V_7 \tag{41g}$$

$$Y_8 = U_o \left(\frac{1 + \underline{u}'}{\cos \underline{\alpha}}\right) V_8 \tag{41h}$$

$$Y_9 = U_o \left[\dot{x}_2 + (1 + x_2) x_4 \tan x_3 + x_3 \sin x_3 - x_4 \sin x_1\right] + V_9 \tag{41i}$$

where x_i is the i^{th} component of the aircraft state vector x defined by equation (6a), x_o and z_o are the current 4D coordinates of the desired glideslope, z_e is the vertical coordinate of the elevation antenna phase center, x_a and z_a are the coordinates of the azimuth antenna phase center in the earth-fixed coordinate system and V_i is the noise introduced by the i^{th} sensor. The earth-fixed coordinate system is referenced to the point where a perpendicular from the elevation antenna phase center crosses the runway centerline. The expressions for the accelerations along z_s and x_s, Y_7 and Y_9 respectively, were obtained by differentiating the corresponding velocities in the earth-fixed coordinates and transforming them back to the stability axes. The slant range, Y_3, and the elevation, Y_4, were obtained for a planar MLS. The values for the standard deviations of the sensor noises were chosen to reflect current instrumentation standards [12], [13]; the values are given in Table 1. The measurements given by equation (41) are then processed by a non-linear transformation given by equation (42) to obtain flight path error signals which are fed into a filter.

$$y_1 = Y_1 - \theta_o - z_1 = e_1 + v_1 \tag{42a}$$

$$y_2 = Y_2 - z_4 = e_4 + v_2 \tag{42b}$$

$$y_3 = -\frac{1}{U_o} (r_e \cos Y_4 + x_o) - z_5 = e_5 + v_3 \tag{42c}$$

$$y_4 = -\frac{1}{U_o}(r_e \sin Y_4 - z_e + z_o) - z_6 = e_6 + v_4 \tag{42d}$$

$$y_5 = \frac{1}{U_o}(z_o - Y_5) - z_6 = e_6 + v_5 \tag{42e}$$

$$y_6 = \frac{1}{U_o}(\sin\gamma_o - Y_6) - E_6' Az = E_6' Ae + v_6 \tag{42f}$$

$$y_7 = \frac{Y_7}{U_o} - E_3' (Bu + Az) = E_3' (Ae + DC_w W) + v_7 \tag{42g}$$

$$y_8 = \frac{Y_8}{U_o} - (1 + z_2) = e_2 - E_1' C_w W + v_8 \tag{42h}$$

$$y_9 = \frac{Y_9}{U_o} - E_2' Az = E_2' (Ae + DC_w W) + v_9 \tag{42i}$$

where

$$r_e = [Y_3^2 - L_e^2 - 2L_e Y_3 \cos(Y_4 + \eta)]^{1/2} \tag{43a}$$

$$\eta = \tan^{-1}\frac{h_{ea}}{x_a}, \quad L_e = \frac{x_a}{\cos\eta}, \tag{43b}$$

h_{ea} is the height of the elevation antenna above the azimuth antenna, r_e is the range of the aircraft from the elevation antenna, E_j is the j^{th} column of the identity matrix, and v_j is a pseudo noise representing the additive noise in the measurement y_j. Thus, we see from equation (42) that y can be expressed in terms of the error vector e and the wind components W.

$$y_k = y(kT) = C_1 e_k + C_2 W_k + v_k, \tag{44}$$

where C_1 and C_2 correspond to the coefficients of e and W in the right-hand-side terms in equation (42). Thus, y_k is a measurement vector which can be expressed as a linear combination of e and W. Now, rewriting (26a) and (12),

$$\dot{e} = Ae + DC_w W + Bu + (A - A_z)z - \zeta \quad , \tag{45a}$$

$$\dot{W} = A_w W + B_w \xi \quad , \tag{45b}$$

it is seen that the flight path error, e, and the wind components, W, can be estimated using a Kalman filter. Since the desired flight path is known z and ζ are not estimated but used as known parameters. Treating the problem as shown in [5], and using the constant Kalman-Bucy gains, we obtain

$$\hat{e}_{k+1} = \phi \hat{e}_k + \Gamma_w \hat{W}_k + \Gamma u_k + \Gamma_z z_k - \zeta_k + F_1 (y_k - C_1 \hat{e}_k - C_2 \hat{W}_k) \tag{46a}$$

$$\hat{W}_{k+1} = \phi_w \hat{W}_k + F_2 (y_k - C_1 \hat{e}_k - C_2 \hat{W}_k) \quad , \tag{46b}$$

where $\hat{e}_k$ and $\hat{W}_k$ are filtered estimates of e_k and W_k respectively given past values of y_k. Thus, the filter provides the estimates of flight path error, $\hat{e}_k$, and wind estimates, $\hat{W}_k$, which along with the desired flight path parameters, z_k and ζ_k, are fed into the control gain equation (40) to obtain the control commands, u_k. A block diagram of the filter is shown in Figure 5. A block diagram of the control law comprising the filter and feedback is shown in Figure 6.

V. RESULTS

To evaluate the performance and capabilities of the control law and filter developed in previous sections for a CTOL aircraft, a digital simulation of a Boeing 737 aircraft was developed. The flight path considered consisted of capturing a steep glideslope (6°) from level flight at 120 knots, following the glideslope to flare altitude and performing flare until touchdown with a nominal touchdown sink rate of 2 ft/sec. Thus, initially the aircraft is in a trim condition for level flight at 120 knots at an altitude of 3,153 ft., aligned with the runway, at a range of 30,000 ft. (1 knot = 0.5144 m/sec; 1 ft. = 0.3048 m).

The simulation includes the aircraft dynamics, wind gusts, steady winds, wind shear, filter, control law, and measurement generation. The aircraft dynamics were simulated using the perturbation model developed in Section II using the aerodynamic characteristics of a Boeing 737 aircraft. The wind conditions were generated using a random gust model with the Dryden spectra (including the effects of gusts on aircraft attitude rates), steady winds, and wind shear using the wind model developed in Section II. From the simulated aircraft position, velocity, attitude and attitude rates the on-board measurements were obtained using the measurement model given by equation (41) with additive or multiplicative sensor errors according to the sensor. The measurements used consist of MLS data at a rate of 10 samples per second, airspeed, barometric altitude and sink rate, attitude, attitude rates and body-mounted accelerometer data. These measurements are processed by a nonlinear preprocessor and then a linear filter with constant coefficients as shown in equations (42) and (46) respectively. The filter outputs the estimates of flight path errors and wind velocities, which are input to the control gain box which generates elevator position, stabilizer rate, and throttle rate commands which are used in controlling the aircraft and to simulate the next point. Thus, the total closed-loop system is simulated.

The simulation developed has the capability of generating various wind conditions, by adjusting the gust levels, the steady wind velocity

and the rate of change of wind velocities for wind shear generation. Sensor noise levels are also input parameters which can be altered. Logic is included in the filter to accommodate MLS dropouts accompanied by MLS flags. The start and stop times of such dropouts are also input parameters. During a MLS dropout, the filter goes into a mode where position is updated without using MLS data while other data is still used. Furthermore, initial flight path errors at the start of glideslope capture and the sampling rate are also input parameters that can be changed to simulate the closed loop response to different conditions.

Simulation runs of flights starting at glideslope capture and ending at touchdown were made under various conditions; these are shown in Figures 7-13. To compare the effects of various wind conditions, sensor errors, and MLS dropouts, a run with the ideal conditions of no measurement noise and no winds was made; this is shown in Figure 7. The aircraft motion for this case is smooth; at glideslope capture the aircraft pitches down and increases its sink rate to acquire the 6° glideslope. The flight path errors settle to zero following the glideslope, which the control surfaces and thrust settle to their steady values for a 6° glideslope. The flight path errors settle to zero following the glideslope, while the control surfaces and thrust settle to their steady values for a 6° glideslope putting the aircraft into a trim condition for the glideslope. At flare the aircraft pitches up, reduces its sink rate and reduces its forward speed slightly as commanded by the desired flight path. To avoid a high sink rate (as required by a steep glideslope) at low altitudes, the flare altitude was set at 200 ft. although flare initiation at lower altitudes provides acceptable flight path performance and touchdown conditions; it is expected that this provides a sufficient period of time and enough altitude for the pilot to react and take over should a failure to engage the flare mode occur; however, a higher flare altitude can easily be obtained by changing the desired flight path parameters. It should also be noted that engaging flare at 200 ft. allows a more gradual and smooth flare maneuver for passenger comfort than a lower

flare altitude would allow. Note that during flare thrust is gradually increased, so that a higher engine pressure ratio is obtained at lower altitudes.

The flight path followed under no wind and no measurement errors shown in Figure 7, is considered to be the nominal flight path as this is the response of the closed loop system under no disturbances. Thus, the nominal touchdown point is 1646 ft. past the runway threshold at a sink rate of 1.93 ft/sec. Thus, touchdown under various wind conditions is compared to these nominal values. However, the 4D horizontal and vertical errors plotted in Figures 7 to 13, are deviations from the desired flight path rather than the nominal flight path shown in Figure 7. The case with no winds but with measurement noise present is shown in Figure 8, where the presence of noise is seen to cause small deviations in the pitch axis. Figure 9 shows the closed loop response to a steady tail wind of 8 ft/sec. and average gust conditions (ζ_u = 2 ft/sec., ζ_w = 1 ft/sec.). It is seen that the wind velocity estimates follow the actual wind velocities; particularly, the total wind velocity has little error. With the steady wind present, the control system retrims the aircraft to follow the desired flight path as can be seen from the pitch attitude.

To see the closed loop response to a wind shear condition, under average gust conditions and errors in the initial estimates, a wind shear condition where a tail wind of 8 ft/sec. (about 5 knots) changes linearly into a 16 ft/sec. (about 10 knots) head wind from 500 ft. altitude to 200 ft. was generated; this condition is shown in Figure 10. It is important to note that, for steep glideslopes, the effect of wind shear on the flight path accuracy is larger than for shallow glideslopes. This is due to the difference in sink rate at constant speed; a steep glideslope results in a higher sink rate, so that the aircraft goes from 500 ft. altitude to 200 ft. in a shorter period of time, and the same change of wind velocity occurs in a shorter period of time. Thus, as far as controlling the aircraft in wind shear is concerned, a 5 knot per hundred feet wind shear on a

6° glideslope has similar effects as an approximately 10 knot per hundred feet wind shear on a 3° glideslope. As can be seen from Figure 10, the wind estimates follow the changing wind, and the control law using this information keeps the flight path errors low; in fact it is difficult to notice that a shear condition is present by looking only at the 4D horizontal and vertical errors; however, control action and changes in the attitude point out the shear condition. It is also interesting to note that at the start of the wind shear, the filter attributes most of the change in wind velocity to fast changing gusts, but as the wind velocity persists in the change, the wind shear estimate follows the change. The total wind in the forward direction, however, is estimated more accurately on an instantaneous basis than its components, and has no noticeable lag; thus, this information can be displayed to the pilot in real time to provide quick warning of changing winds.

To see the effects of an MLS dropout condition, a 10 second dropout condition characterized by bad flags output by the on-board MLS receiver was simulated; this case is shown in Figure 11. Thus, from 30 sec. to 40 sec. the filter operates in a mode which does not use MLS data but updates position estimates using the other sensor data such as body-mounted accelerometer and air data. The wind conditions correspond to a tail wind of 8 ft/sec. and average gust levels. It is seen from the plots that the filter can update position without significant flight path error for a 10 second period during an MLS fade. Figures 12 and 13 show the cases where the gust levels are high (ζ_u = 4 ft/sec., ζ_w = 2 ft/sec.) with a tail wind, with and without a wind shear condition. Table 2 shows the touchdown condition for the various runs.

VI. SUMMARY AND CONCLUSIONS

In the preceeding sections, a digital automatic longitudinal control law for steep glideslope capture, flare to touchdown was developed using guidance data from the Microwave Landing System. The system uses MLS data, body-mounted accelerometer data, air data, attitude and attitude rate data to compute the control surface commands for automatic landing. The control law is developed to accommodate turbulence and wind shear whose effect is magnified for steep glideslopes. The filter used filters out the noise in the received data and computes estimates of the wind velocities which are used to generate control commands under the estimated wind conditions to follow the desired flight path.

A digital simulation of the aircraft and the control law was developed for use in a partial evaluation of the system developed. The simulation includes the longitudinal aircraft dynamics for a 6° glideslope, wind conditions in terms of gusts, steady winds and wind shear, sensor outputs with noise, filter and controller. As a partial evaluation of the performance of the system a limited number of runs to simulate various conditions were made. The flight path tracking performance evaluated by flight path errors show only small deviations on the glideslope and quick response in capturing the steep glideslope; the touchdown conditions show no excessive sink rates corresponding to "hard" landings, and no excessive touchdown dispersion. The wind estimates computed by the filter follow the wind velocities and changes in the wind velocities; wind shear conditions are detected through large and lasting changes in the wind velocity estimates. Thus, the simulation results indicate that the techniques presented can be used to perform automatic steep approaches with MLS guidance. For a more complete evaluation of the system developed, use of non linear aircraft dynamics coupled with a lateral control law for crab and decrab maneuvers would be required.

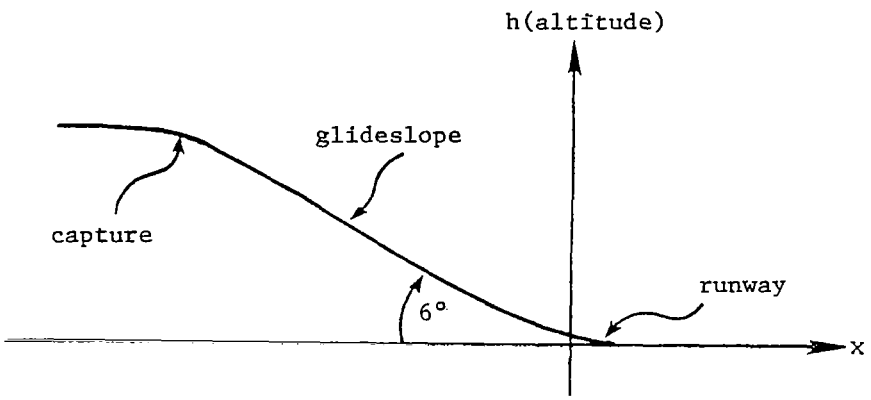

Figure 1 Flight Path for Capture and Glideslope

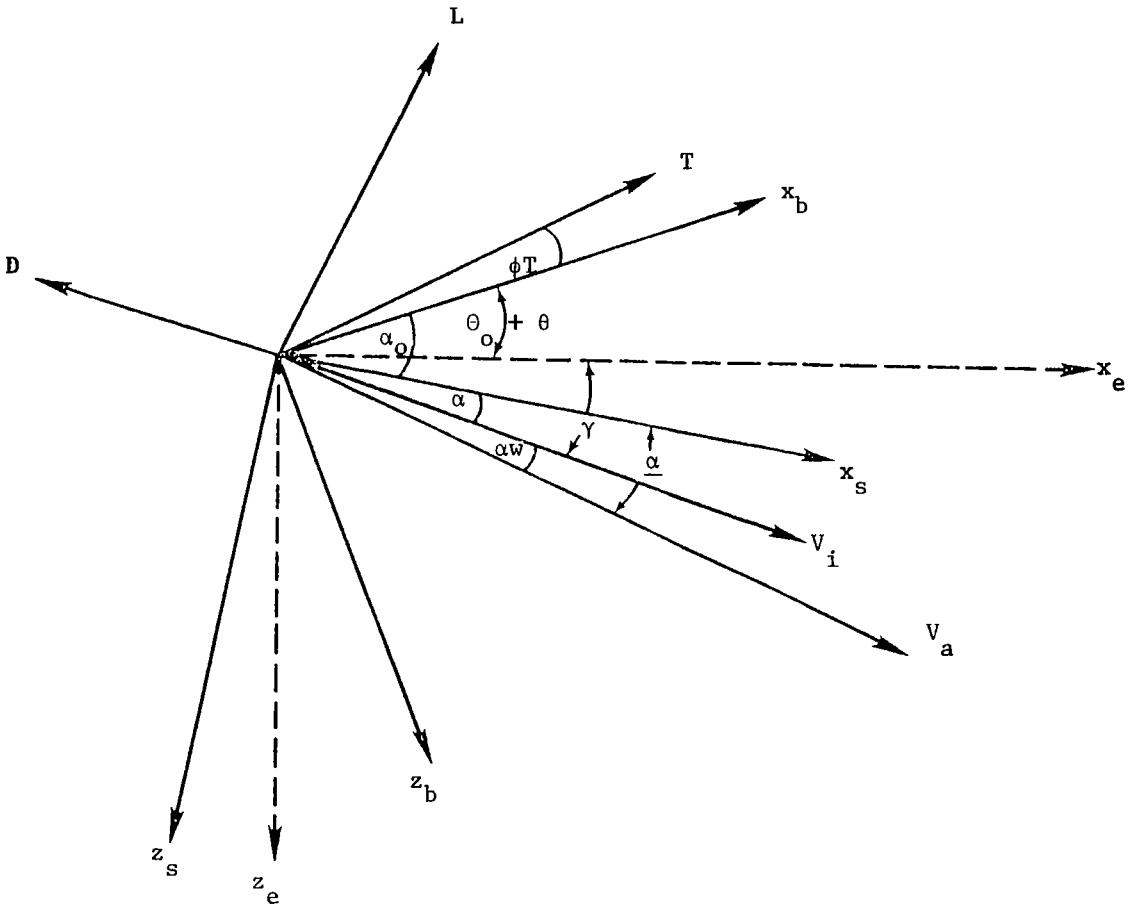

Figure 2 Definition of coordinate axes, angles and forces. (Θ_o, θ ϕ_T are measured positive ccw, α_o, α_w, $\underline{\alpha}$, cw)

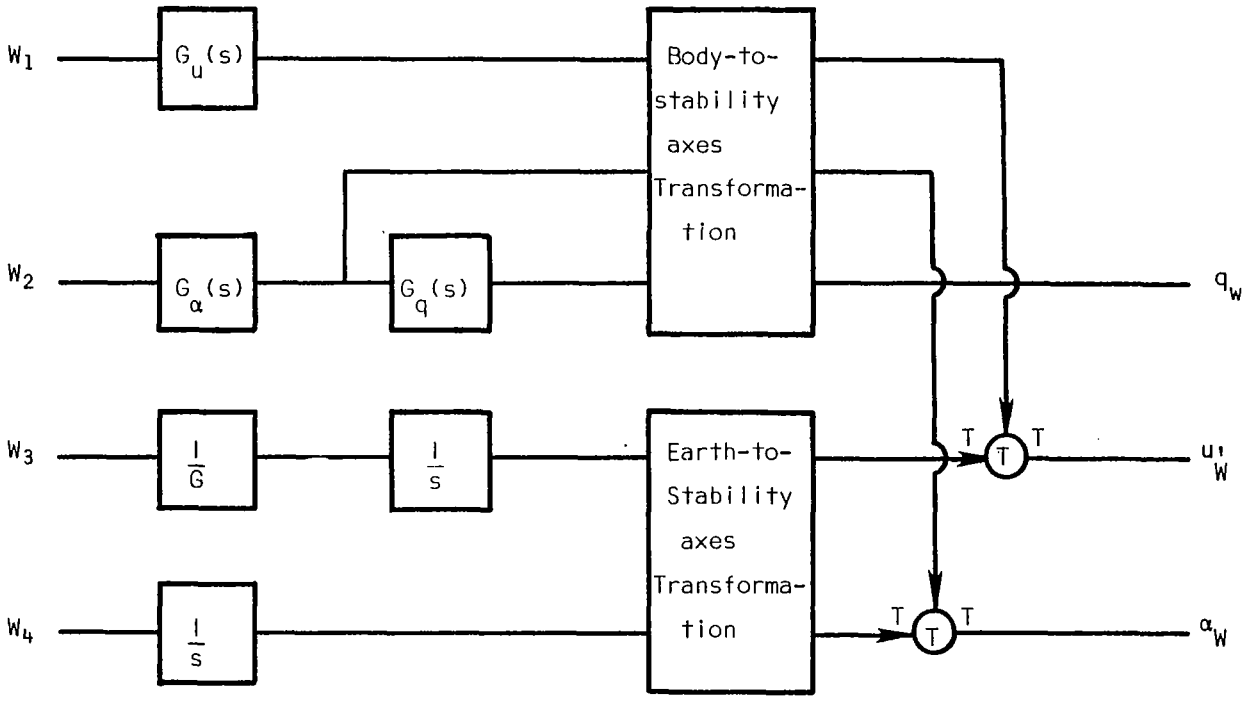

Figure 3 Wind Model Block Diagram

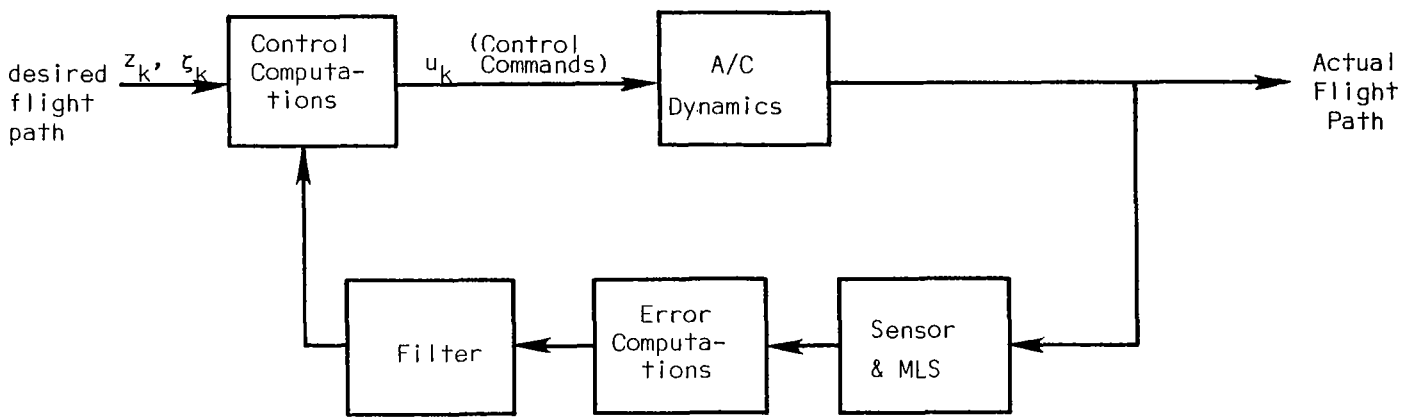

Figure 4 Functial Block Diagram
of Closed Loop System

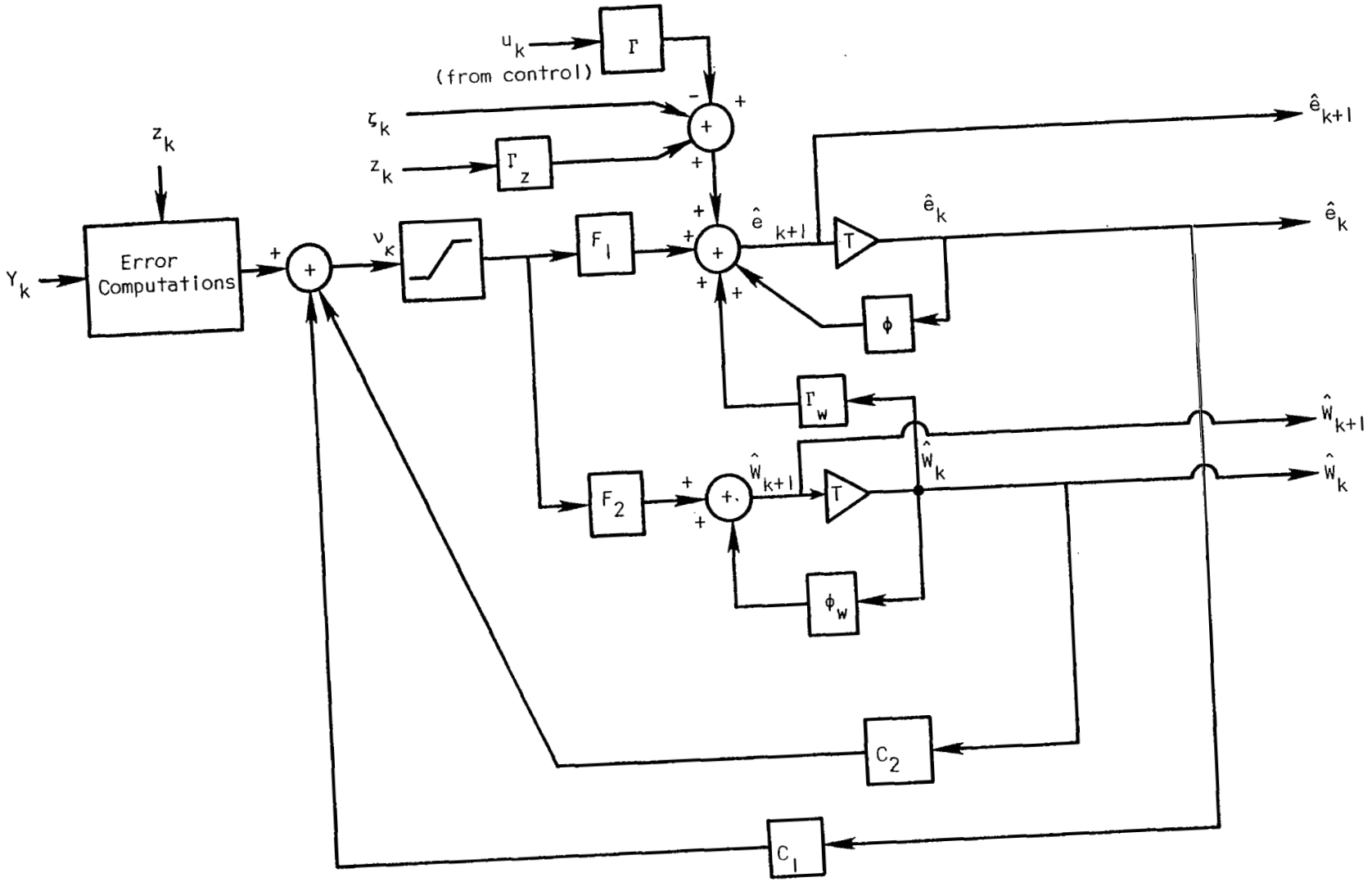

Figure 5 Filter Block Diagram

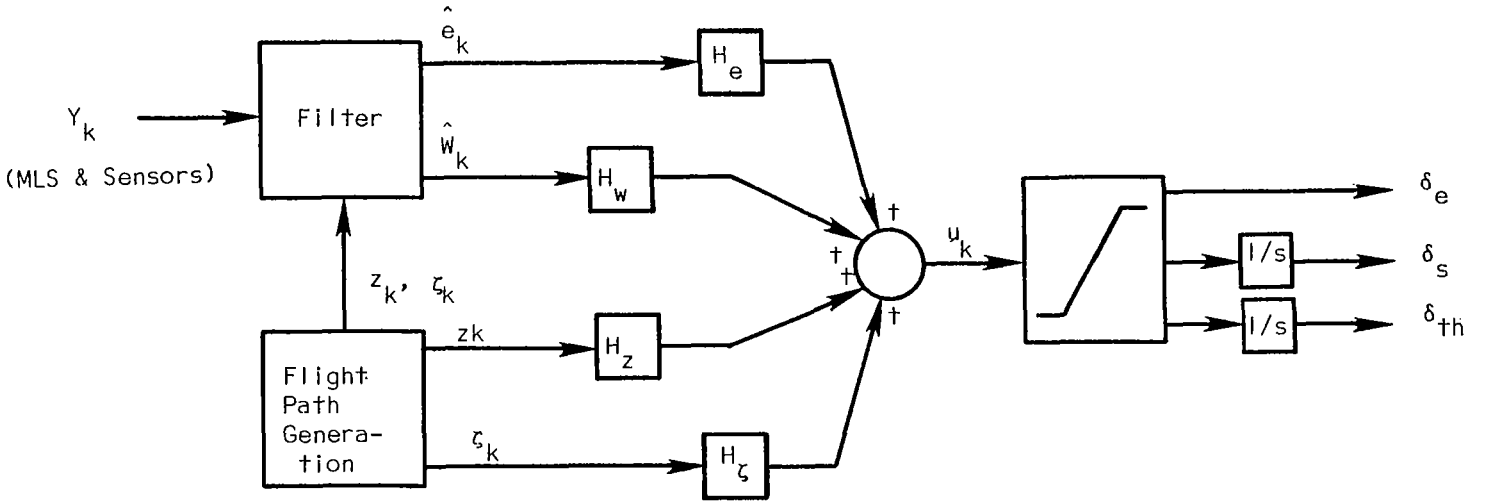

Figure 6 Block Diagram of Feedback Loop

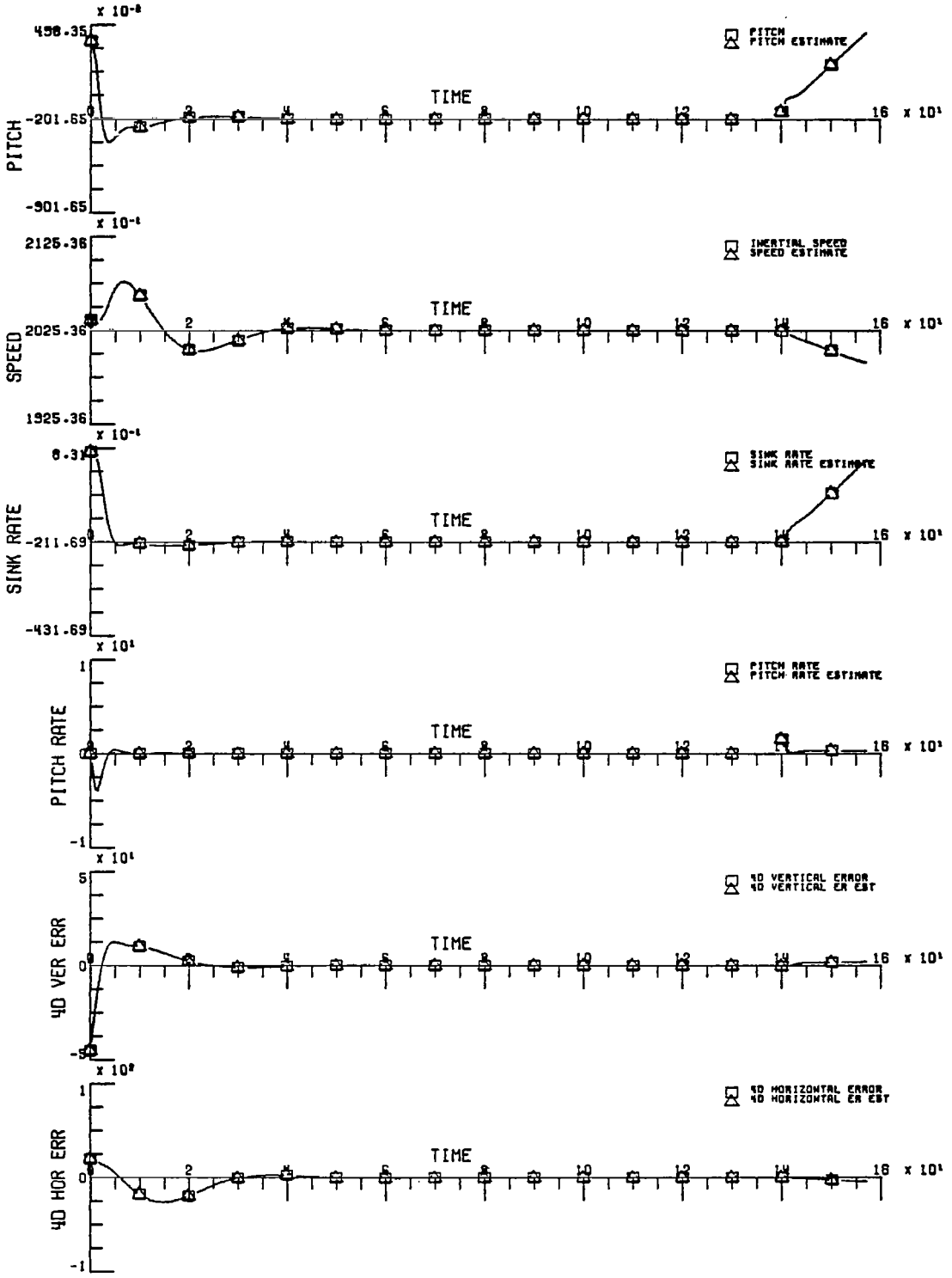

Figure 7A Closed Loop Responses Simulation:
No Measurement Noise, No Winds
(1 ft. = 0.3048 m).

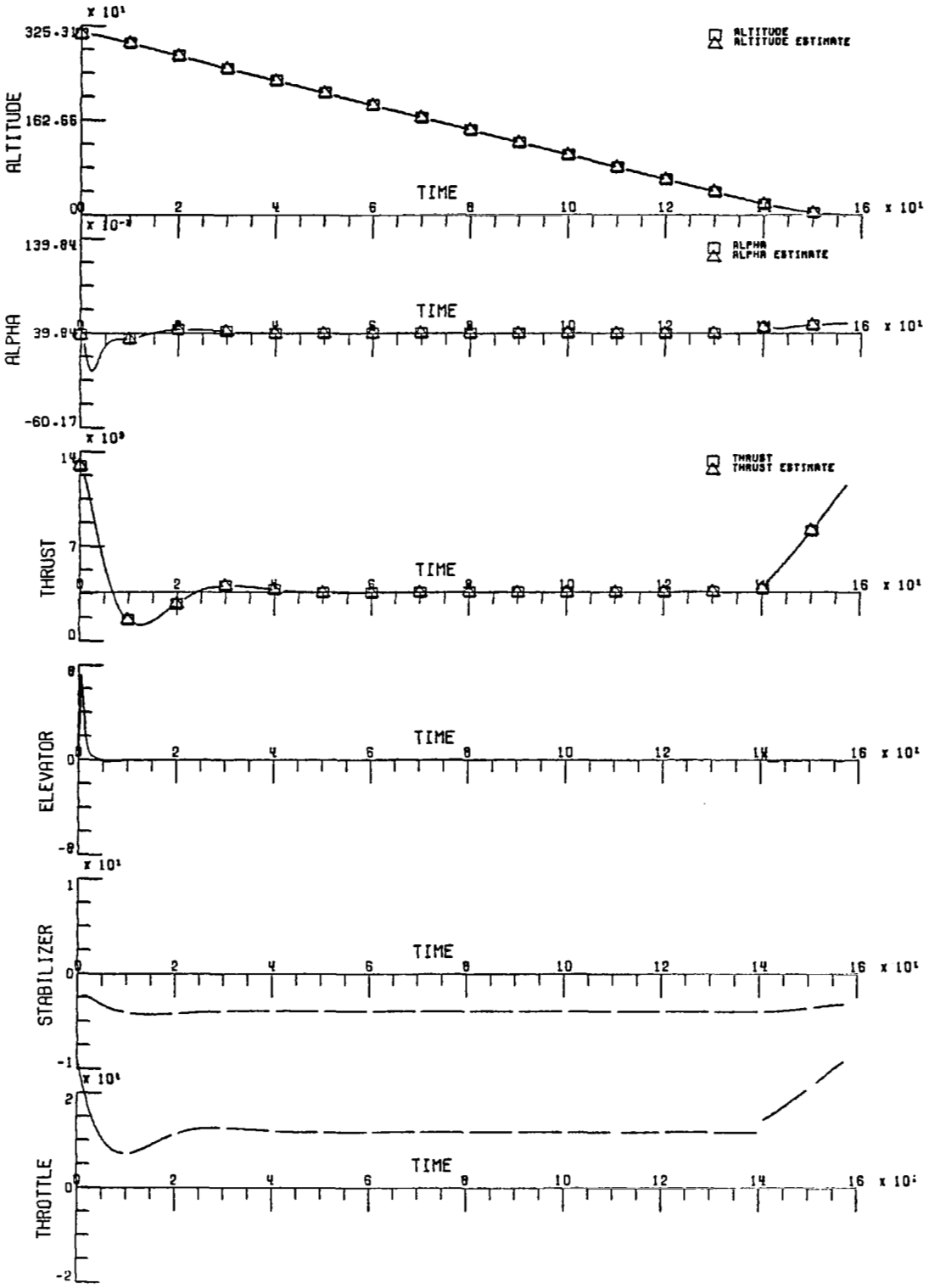

Figure 7B Closed Loop Responses Simulation:
No Measurement Noise, No Winds
(1 ft. = 0.3048 m; 1 lb = 4.448 N).

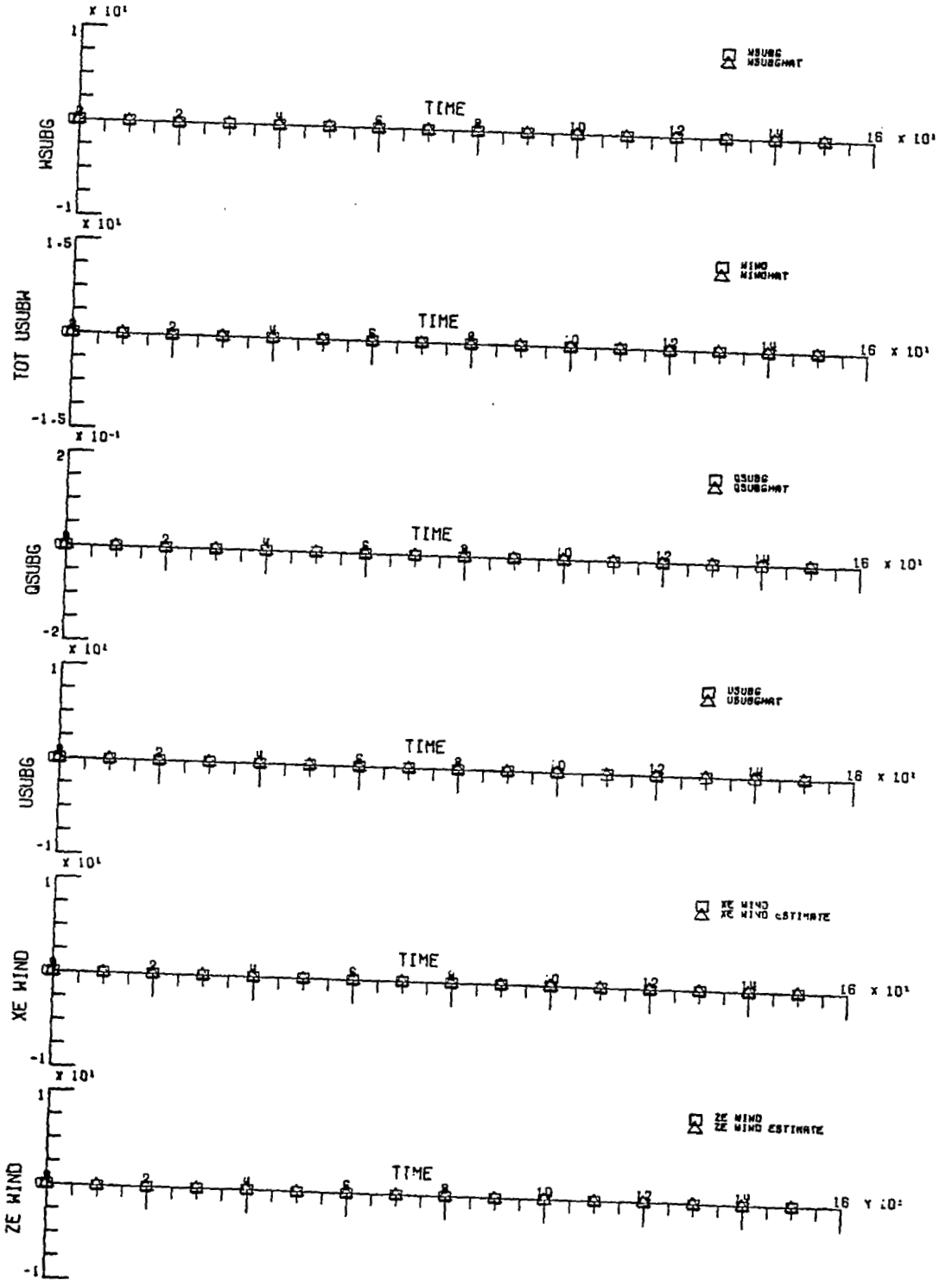

Figure 7C Closed Loop Responses Simulation:
No Measurement Noise, No Winds
(1 ft. = 0.3048 m)

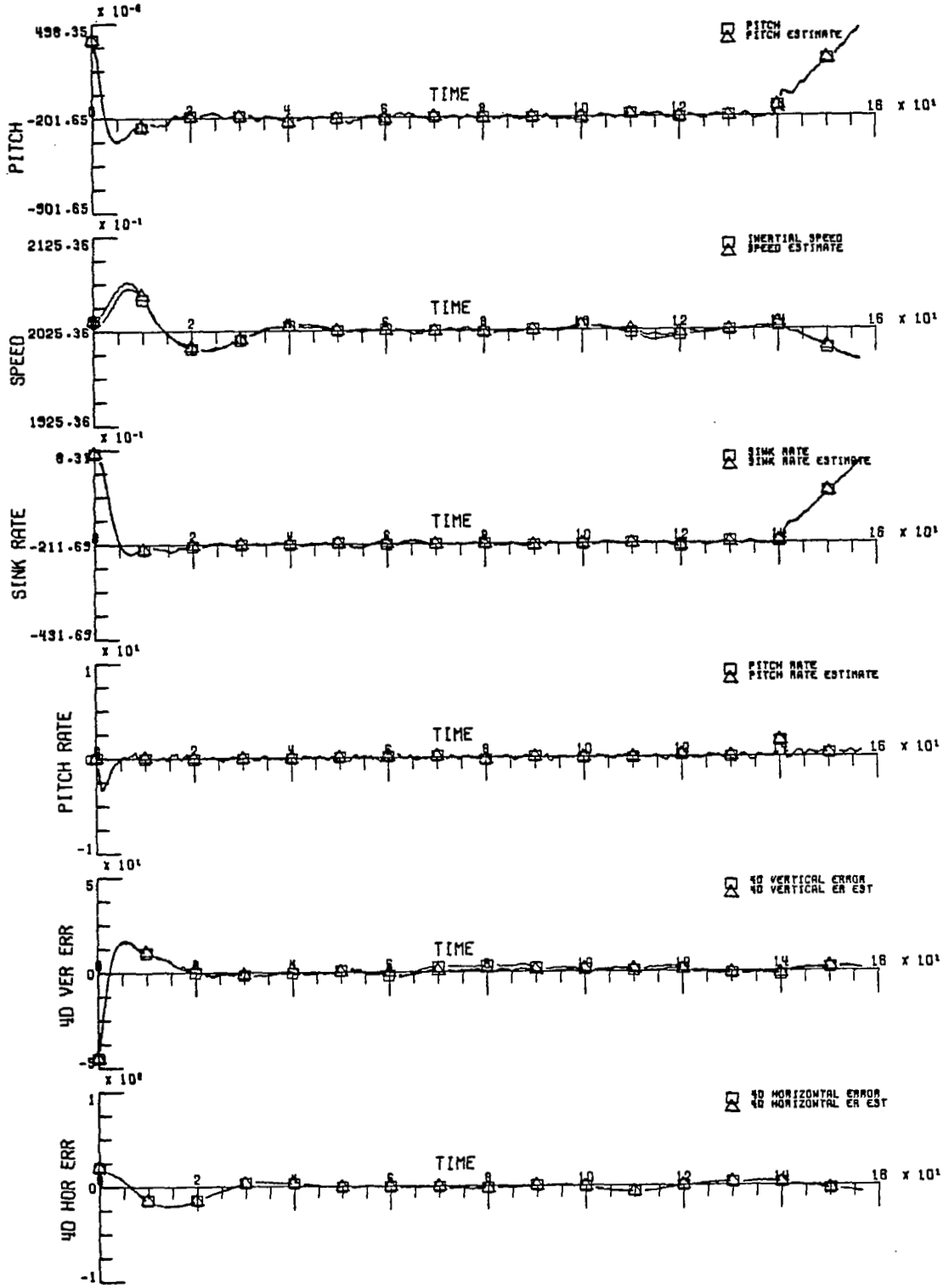

Figure 8A Closed Loop Response Simulation:
Meas. Noise Present, No Winds
(1 ft. = 0.3048 m).

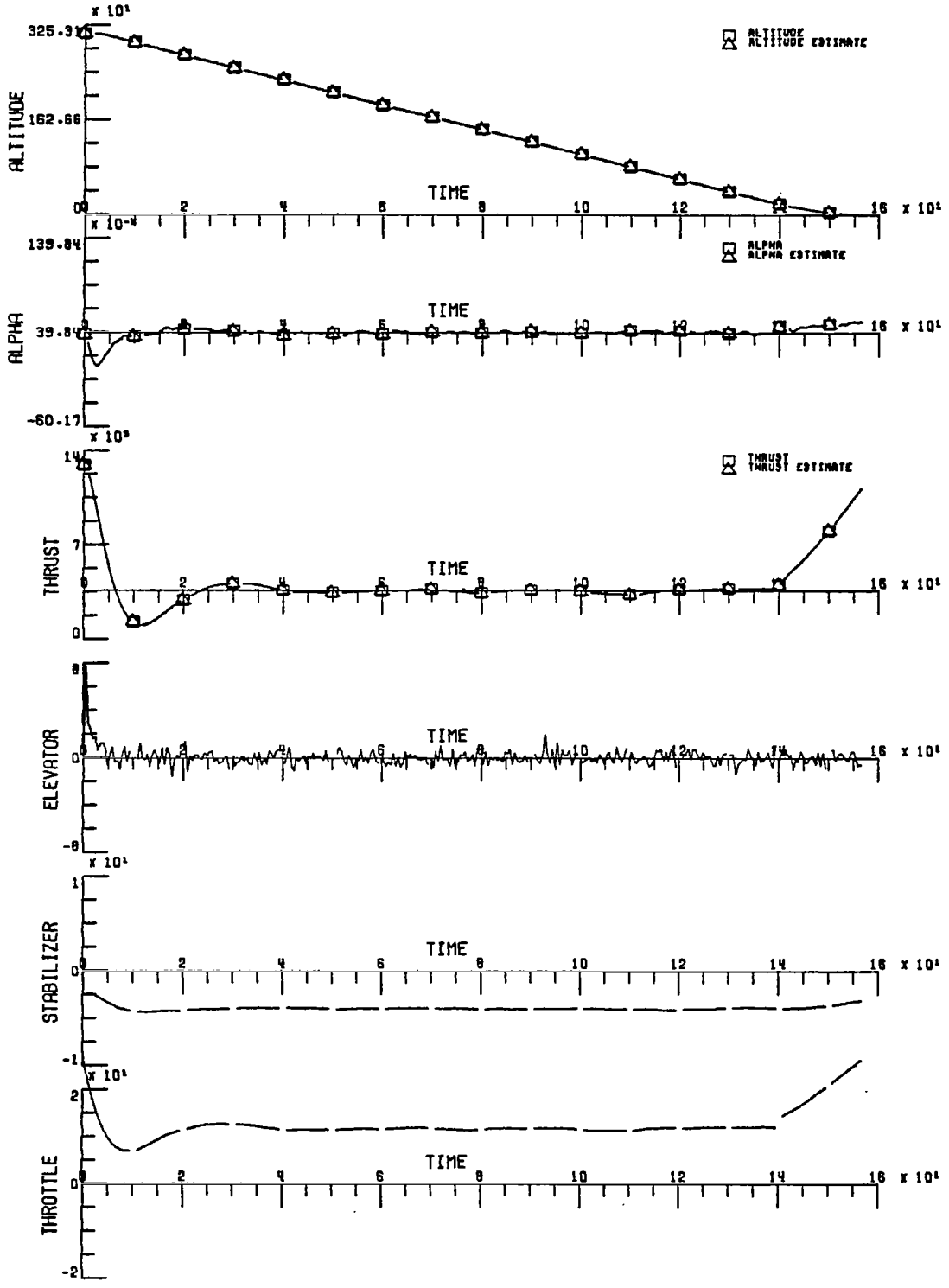

Figure 8B Closed Loop Response Simulation:
Meas. Noise Present, No Winds
(1 ft. = 0.3048 m; 1 lb. = 4.448 N).

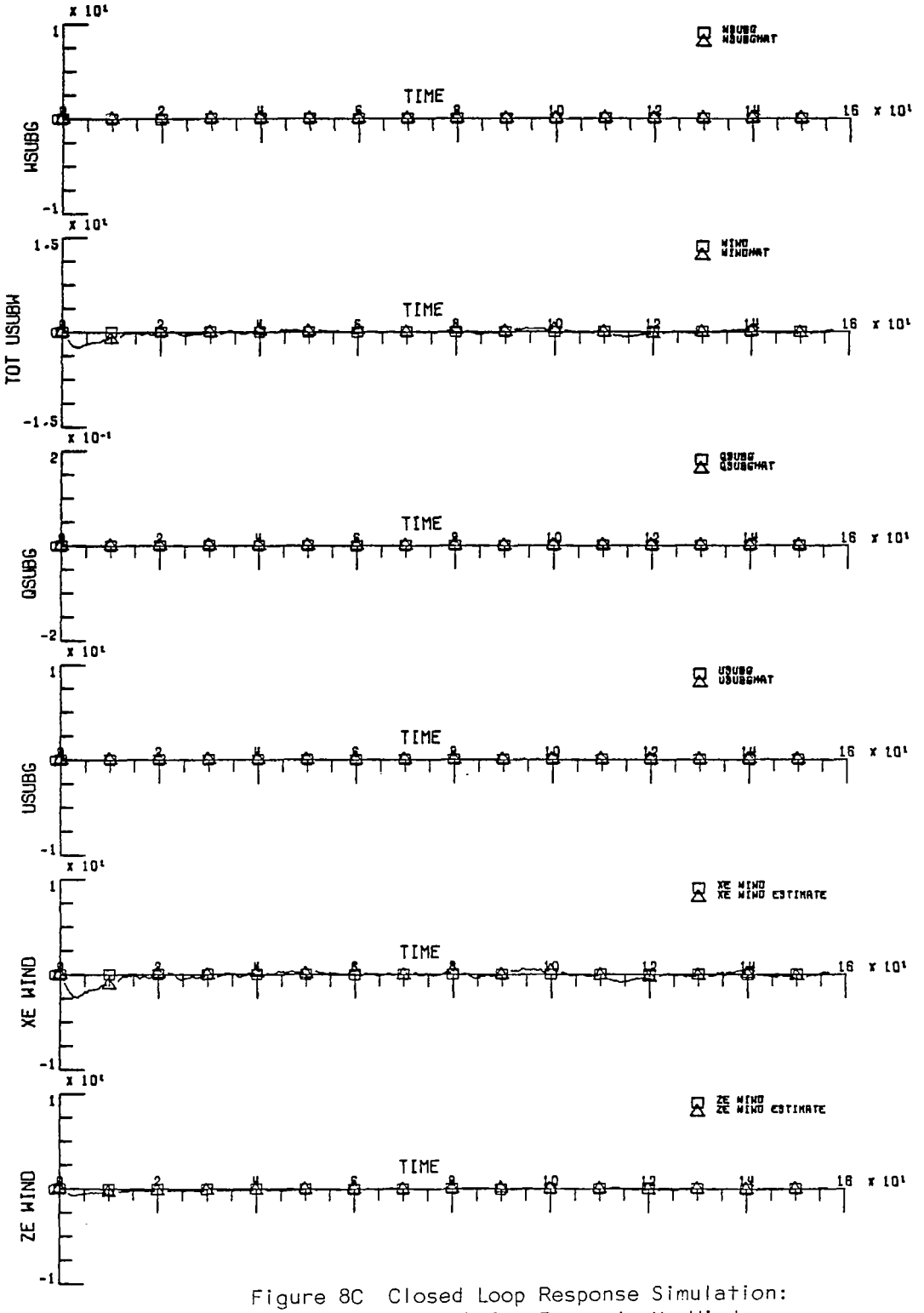

Figure 8C Closed Loop Response Simulation:
Meas. Noise Present, No Winds
(1 ft = 0.3048 m)

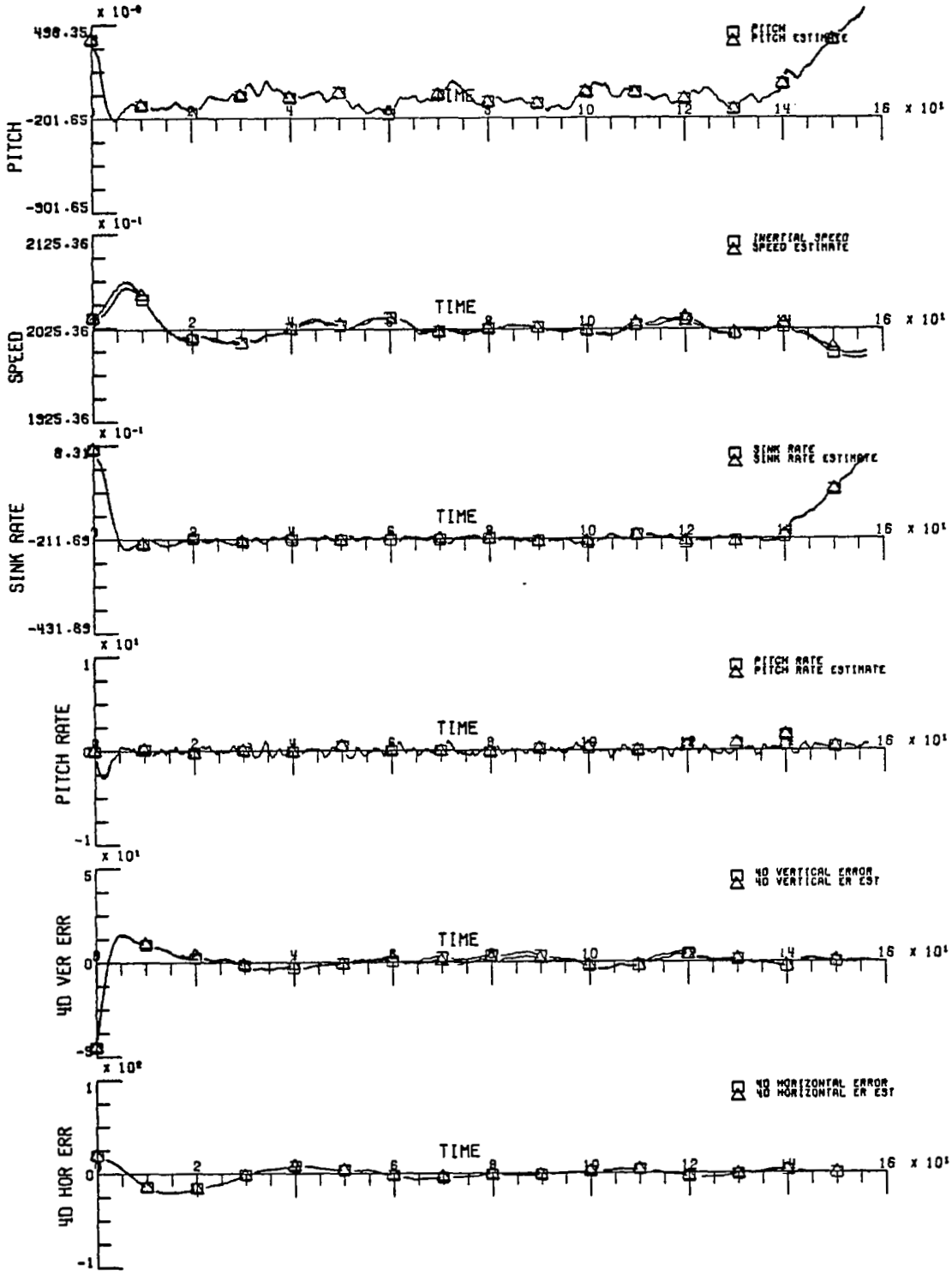

Figure 9A Closed Loop Response Simulation: Meas. Noise Present, 8 ft/sec. Tail Wind, Average Gusts (τ_u = 2 ft/sec., τ_w = 1 ft/sec.) (1 ft = 0.3048 m)

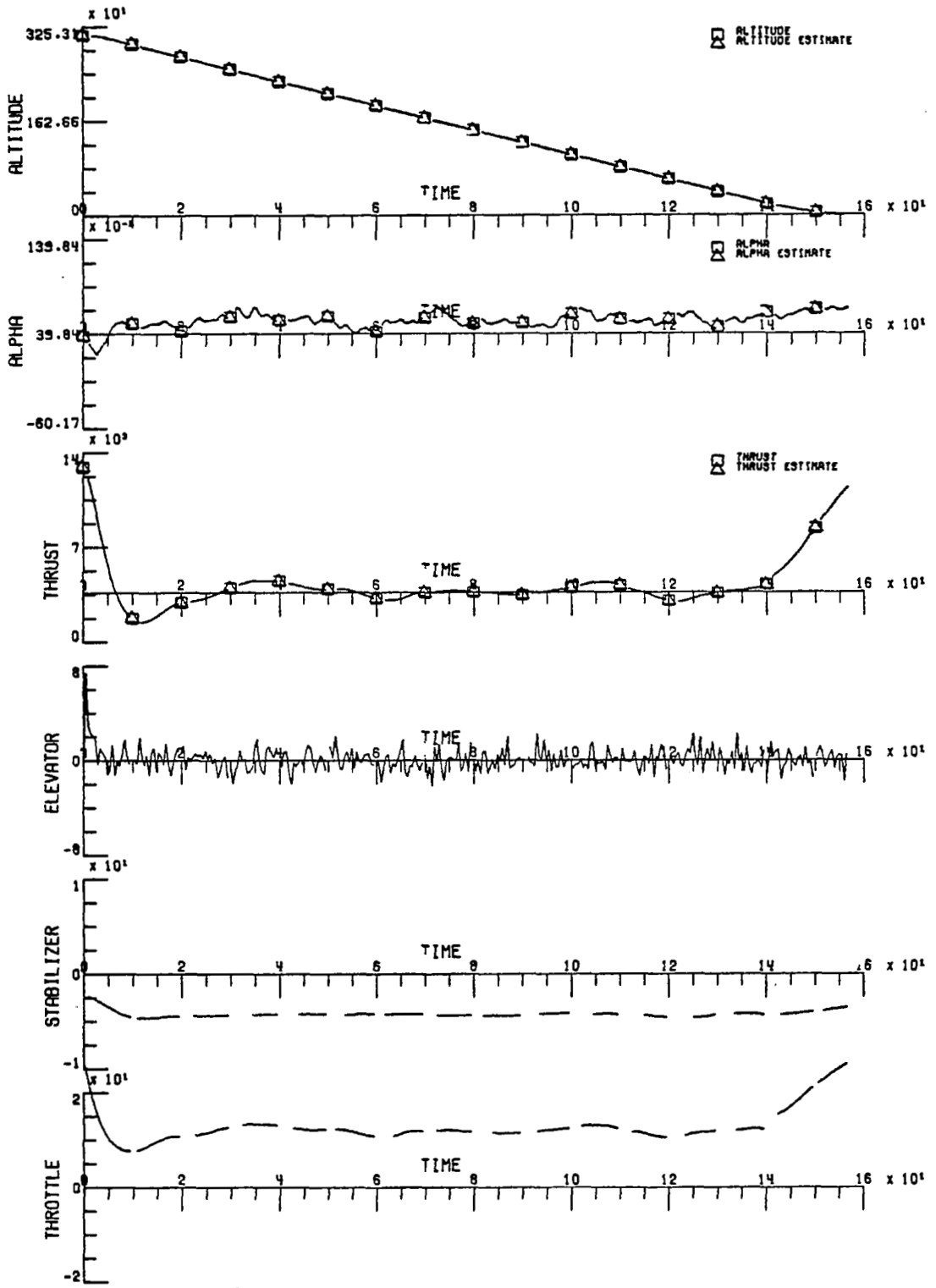

Figure 9B Closed Loop Response Simulation: Meas. Noise Present, 8 ft/sec. Tail Wind, Average Gusts (τ_u = 2 ft/sec., τ_w = 1 ft/sec.) (1 ft. = 0.3048 m; 1 lb. = 4.448 N).

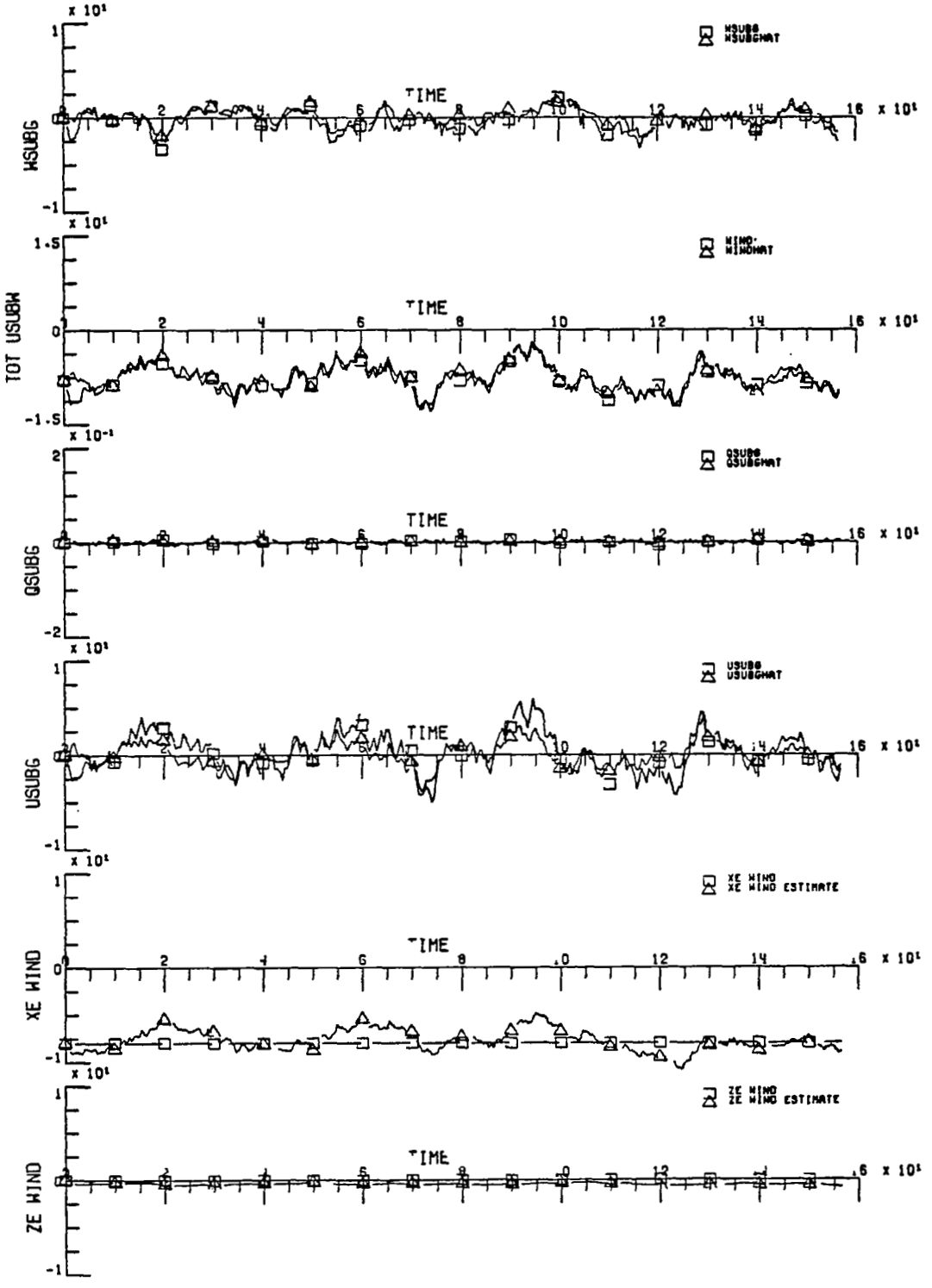

Figure 9C Closed Loop Response Simulation: Meas. Noise Present 8 ft/sec. Tail Wind, Average Gusts (τ_u = 2 ft/sec. τ_w = 1 ft/sec.) (1 ft. = 0.3048 m).

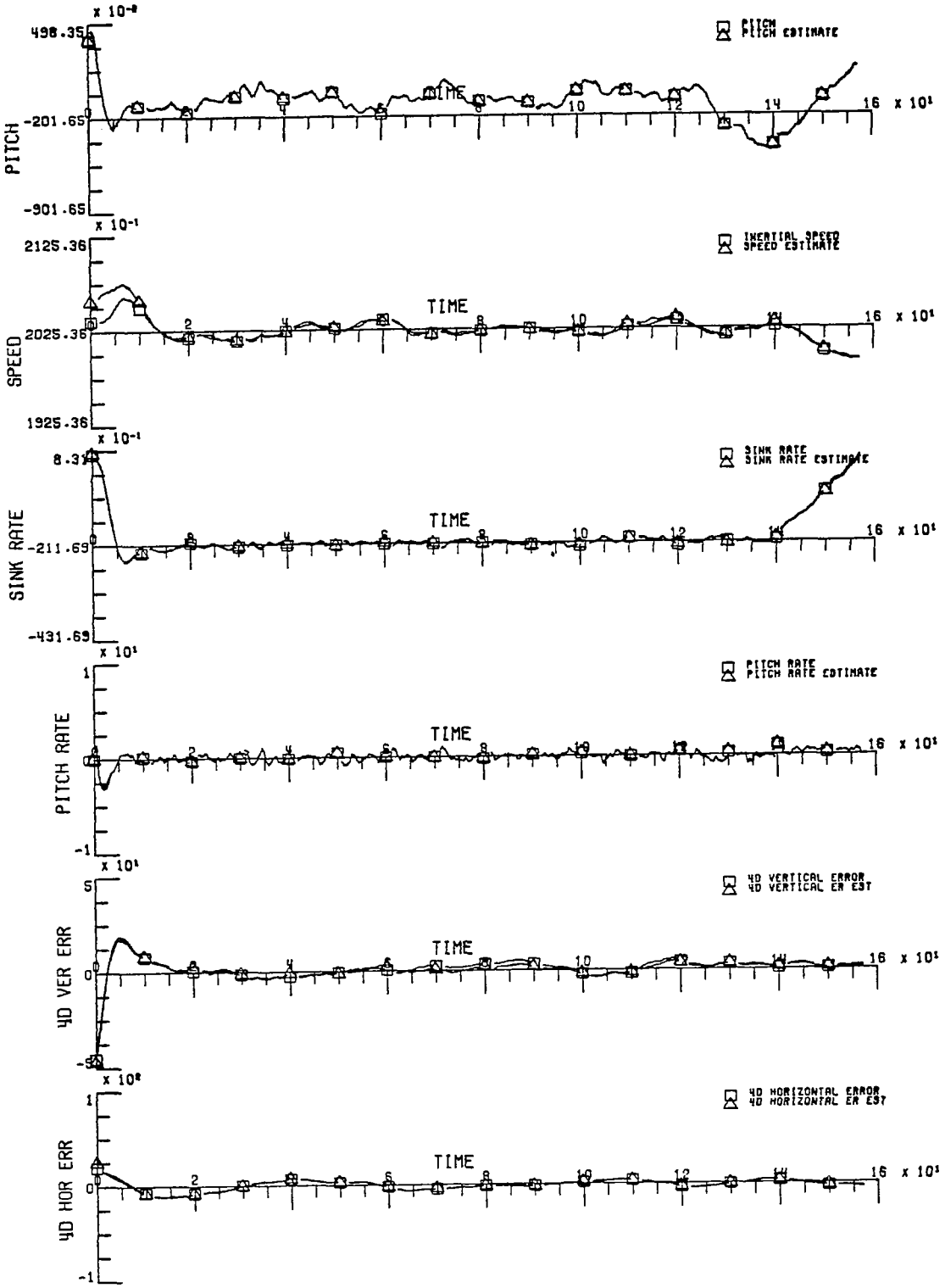

Figure 10A Closed Loop Response Simulation: Meas. Noise Present, Average Gusts (τ_u = 2 ft/sec., τ_w = 1 ft/sec.), Wind Shear of 8 ft/sec. per 100 ft. (1 ft. = 0.3048 m).

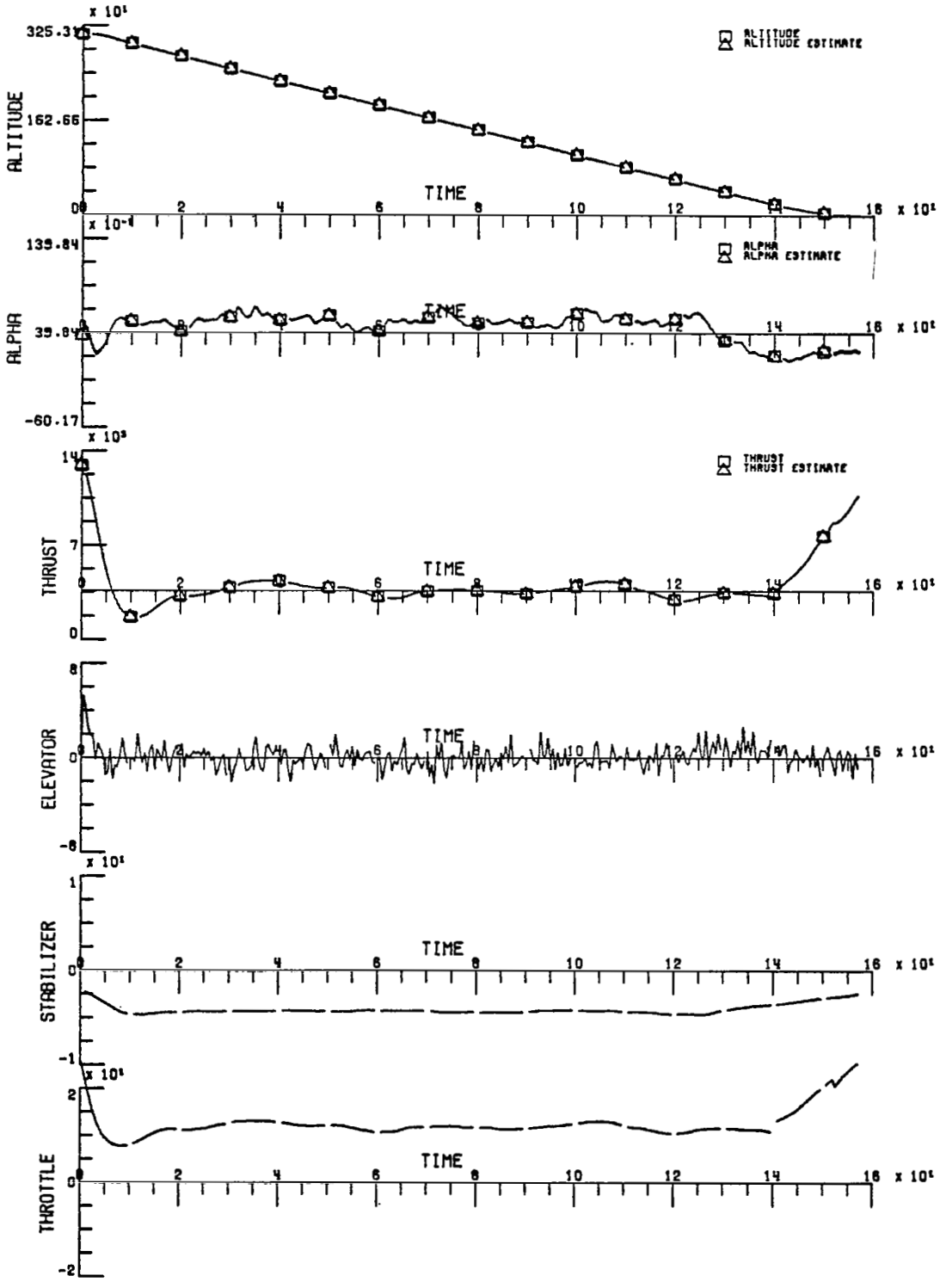

Figure 10B Closed Loop Response Simulation: Meas. Noise Present, Average Gusts (τ_u = 2 ft/sec., τ_w = 1 ft/sec.), Wind Shear of 8 ft/sec. per 100 ft. (1 ft. - 0.3048 m; 1 lb. = 4.448 N).

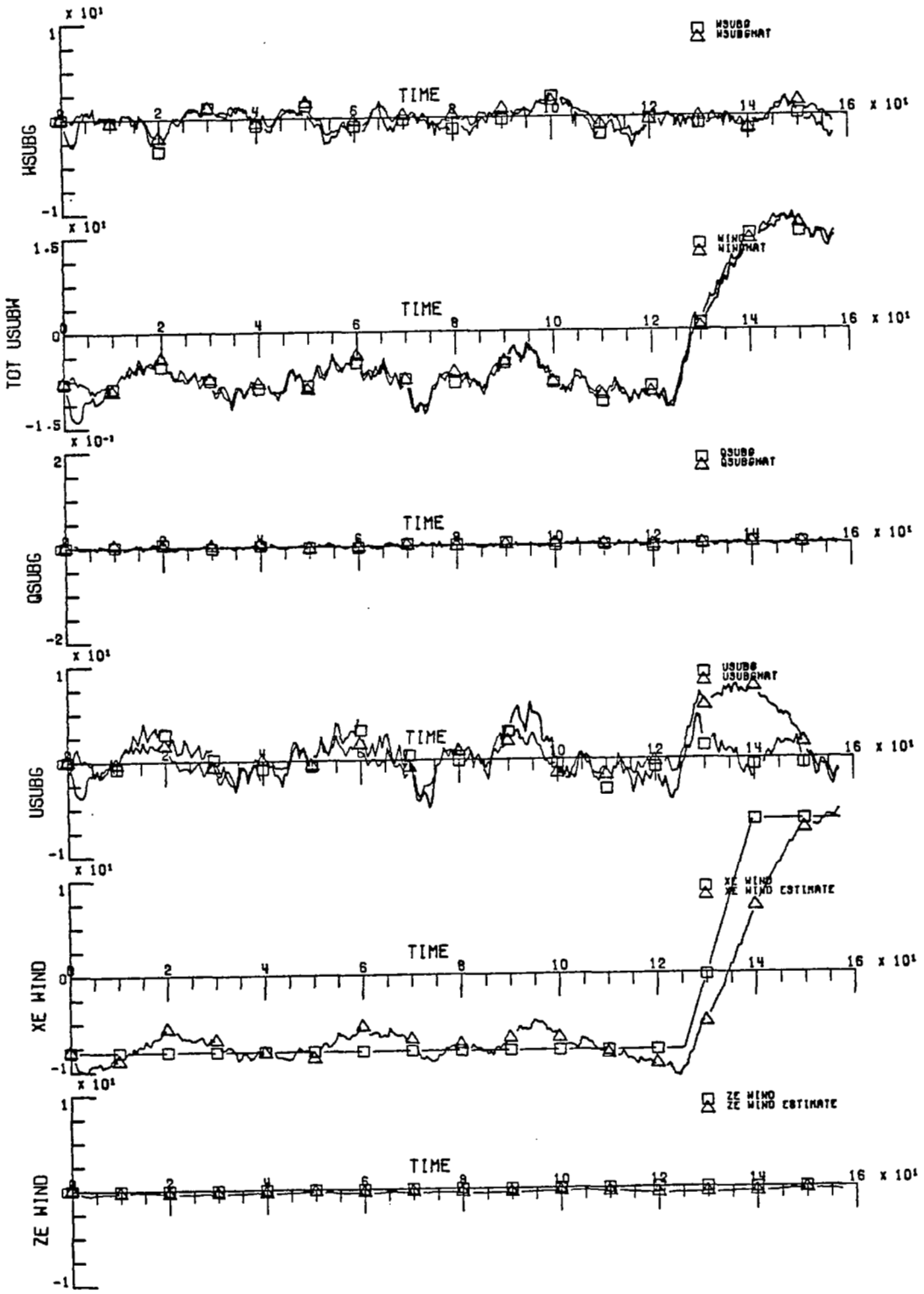

Figure 10C Closed Loop Response Simulation: Meas. Noise Present, Average Gusts (τ_u = 2 ft/sec., τ_w = 1 ft/sec.), Wind Shear of 8 ft/sec. per 100 ft. (1 ft. = 0.3048 m).

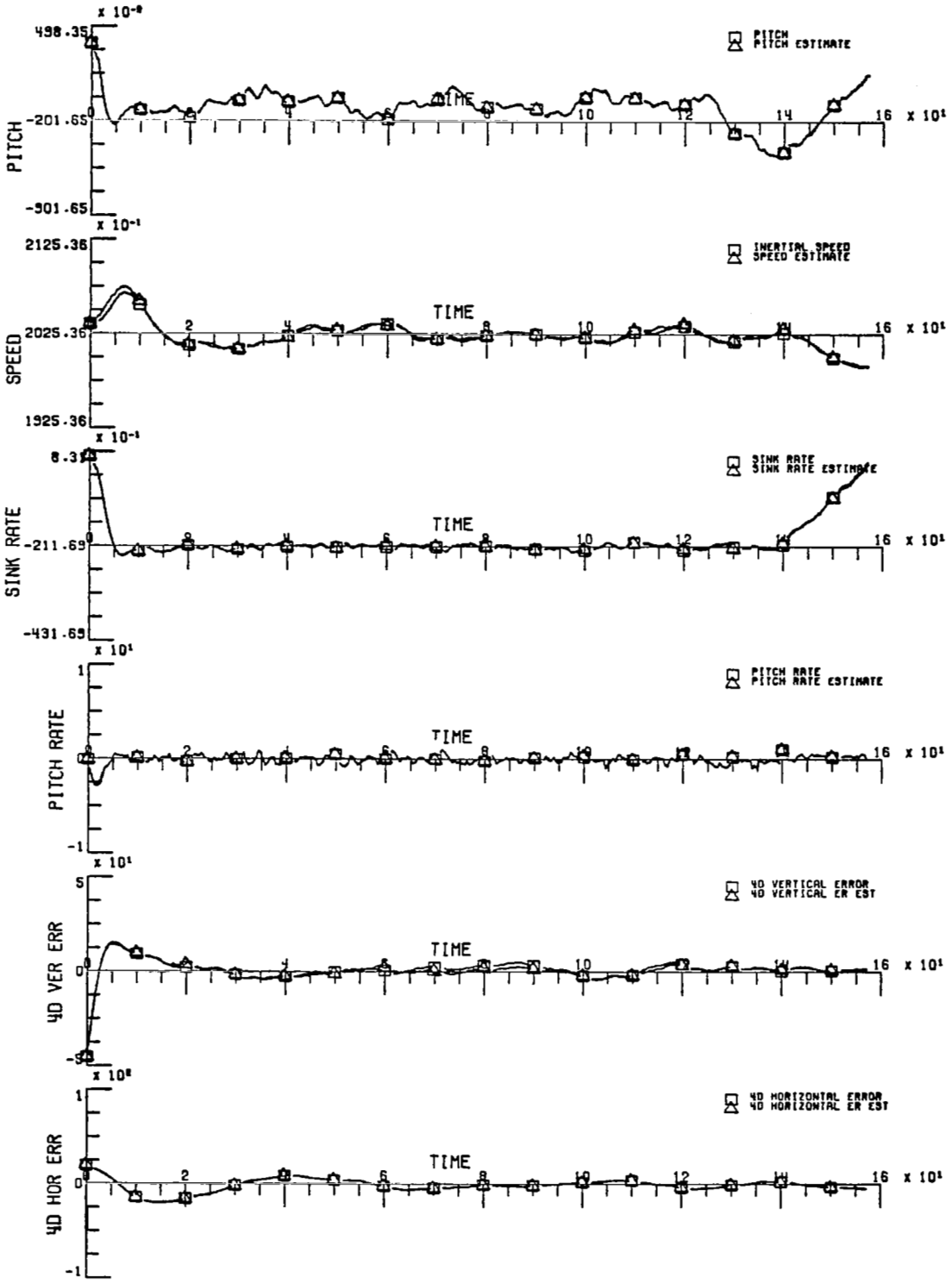

Figure IIA Closed Loop Response Simulation: Meas. Noise Present, Average Gusts, Wind Shear of 8 ft/sec. per 100 ft., 10 sec MLS Fade (1 ft. = 0.3048 m).

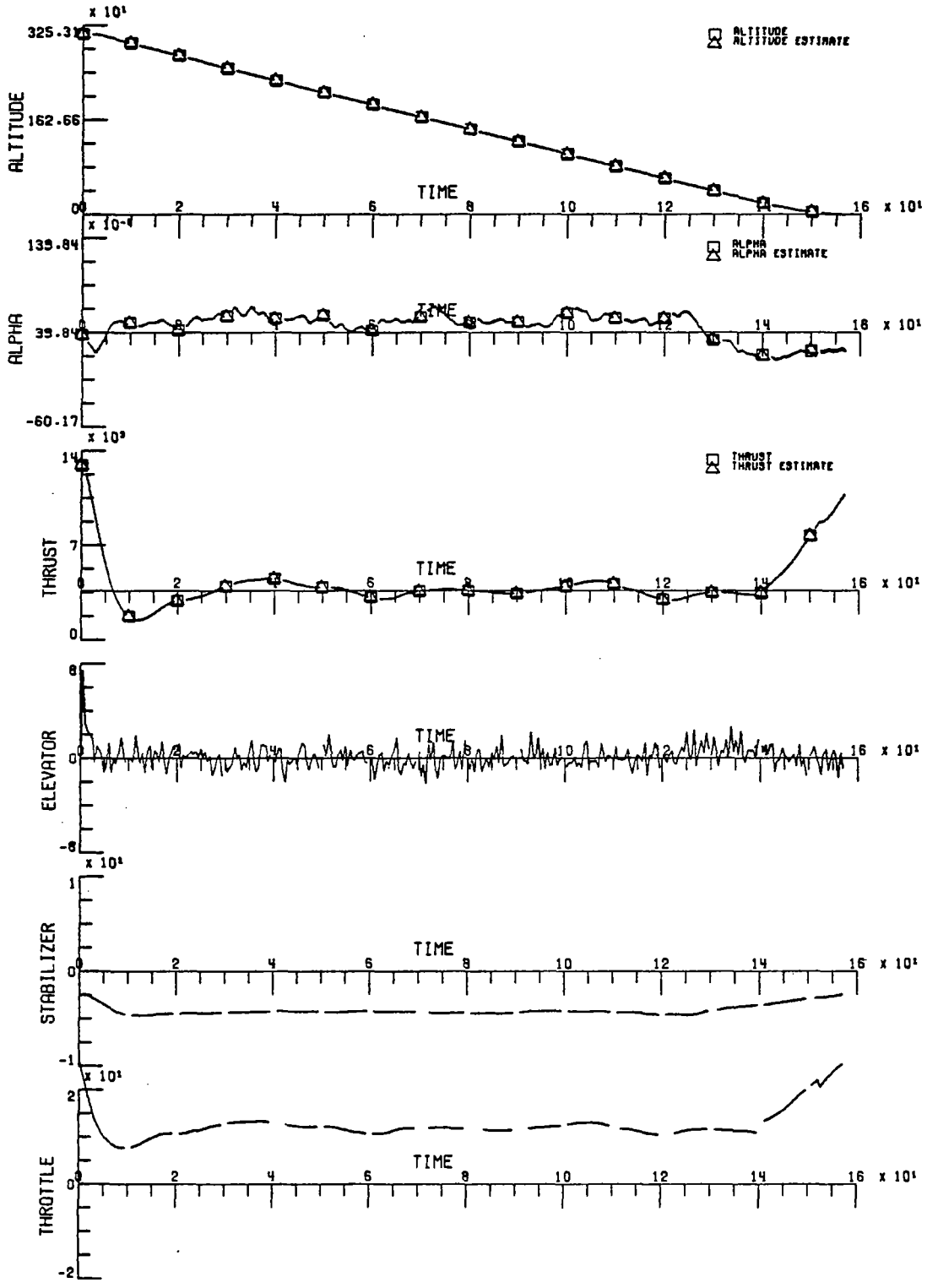

Figure 11B Closed Loop Response Simulation: Meas. Noise Present, Average Gusts, Wind Shear of 8 ft/sec. per 100 ft., 10 sec. MLS Fade (1 ft. = 0.3048 m; 1 lb. - 4.448 N).

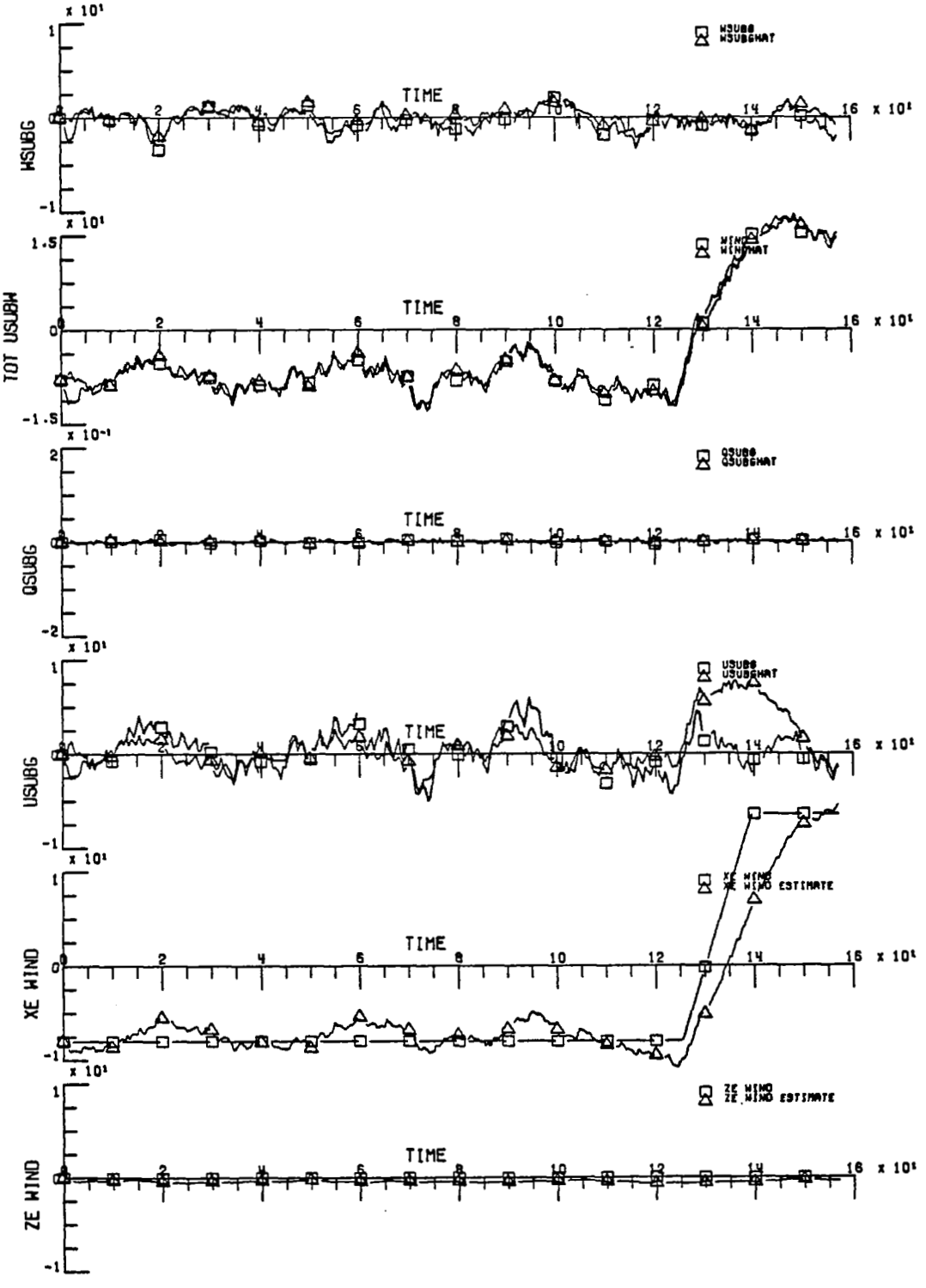

Figure 11C Closed Loop Response Simulation: Meas. Noise Present, Average Gusts, Wind Shear of 8 ft/sec. per 100 ft., 10 sec. MLS Fade (1 ft. = 0.3048 m).

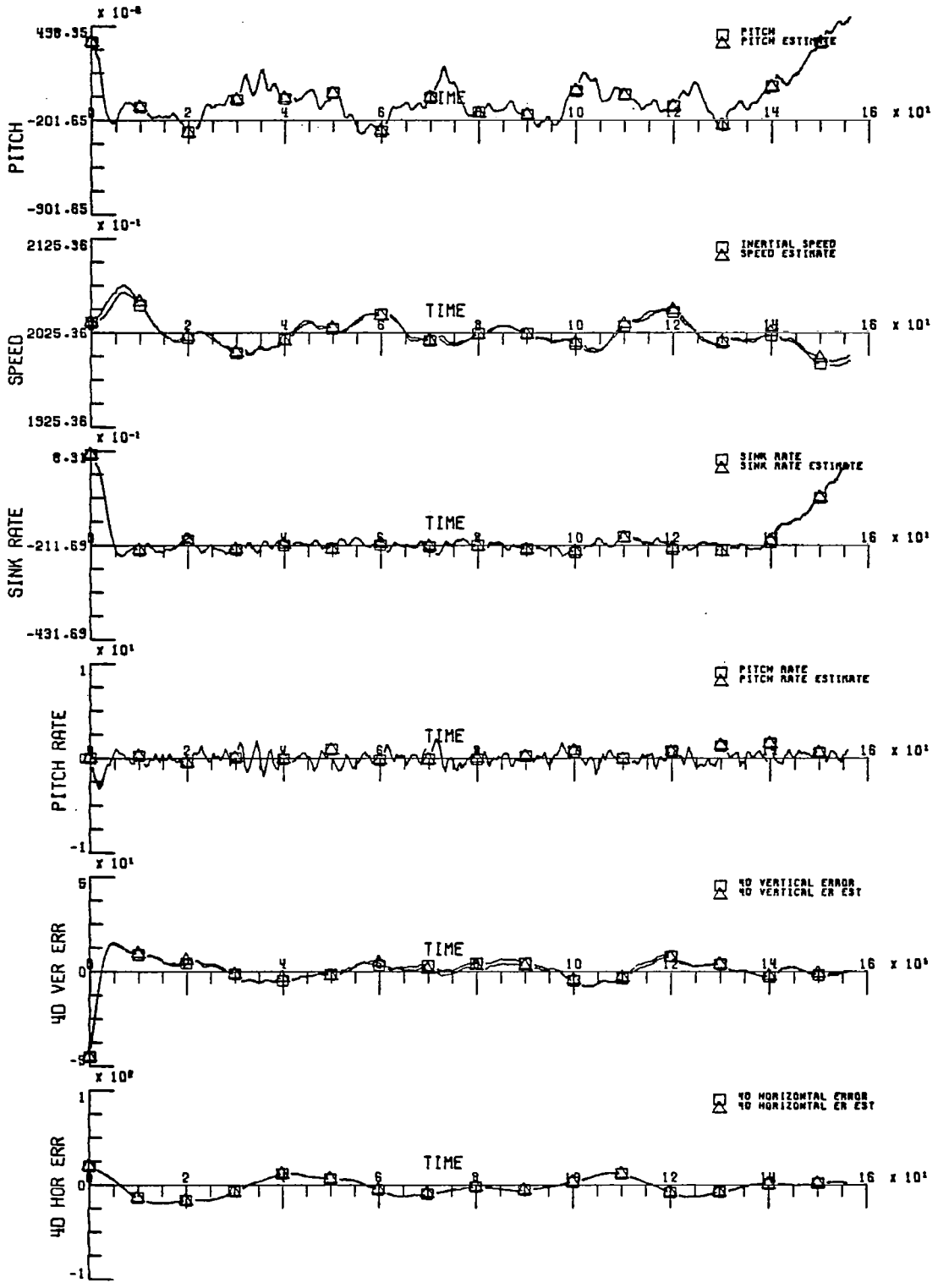

Figure 12A Closed Loop Response Simulation: Meas. Noise Present, High Gusts (τ_u = 4 ft/sec., τ_w = 2 ft/sec.), 8 ft/sec. Tail Wind (1 ft. = 0.3048 m).

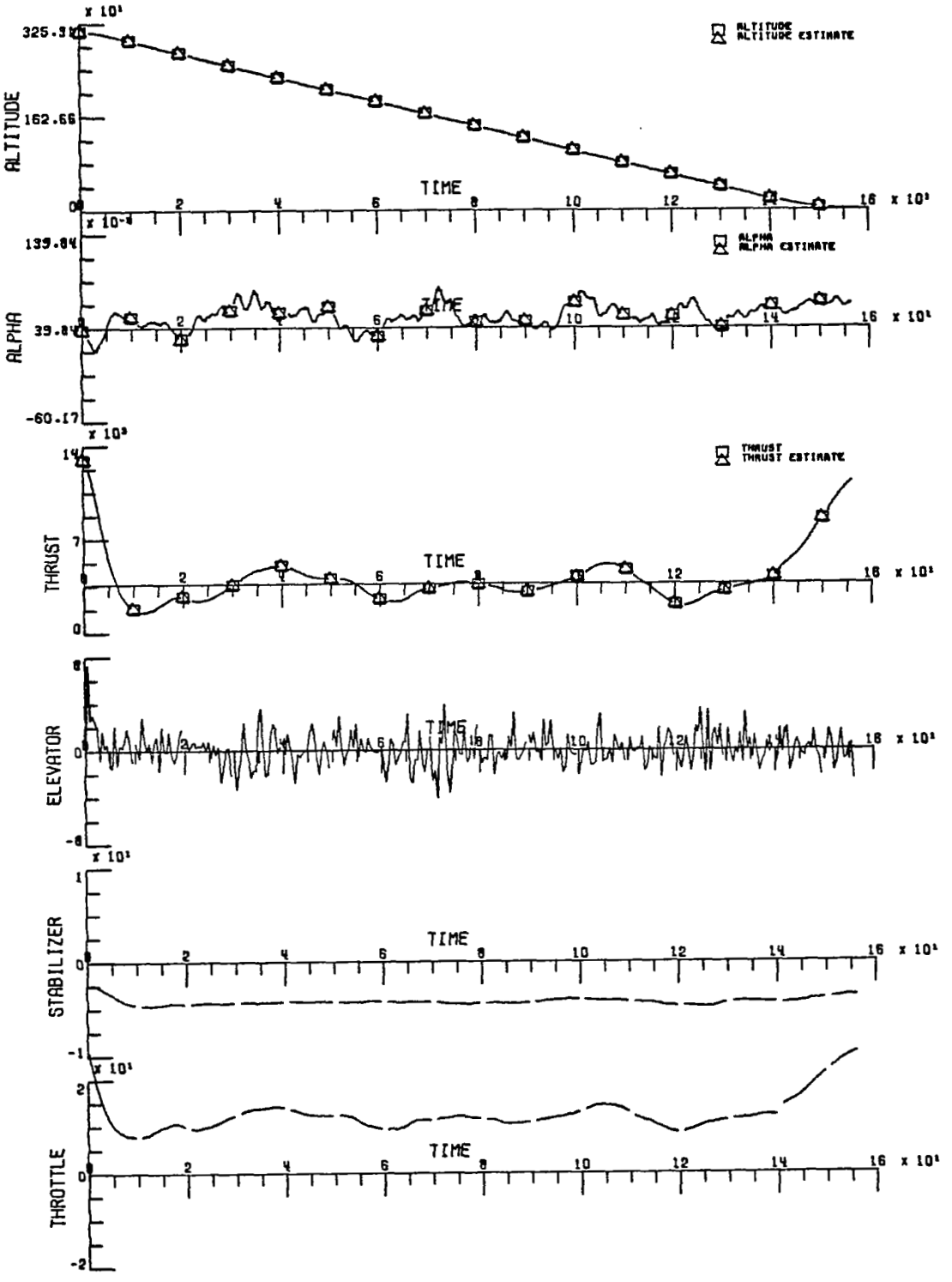

Figure 12B Closed Loop Response Simulation: Meas. Noise Present, High Gusts (τ_u = 4 ft/sec., τ_w = 2 ft/sec.), 8 ft/sec. Tail Wind (1 ft. = 0.3048 m; 1 lb. = 4.448 N).

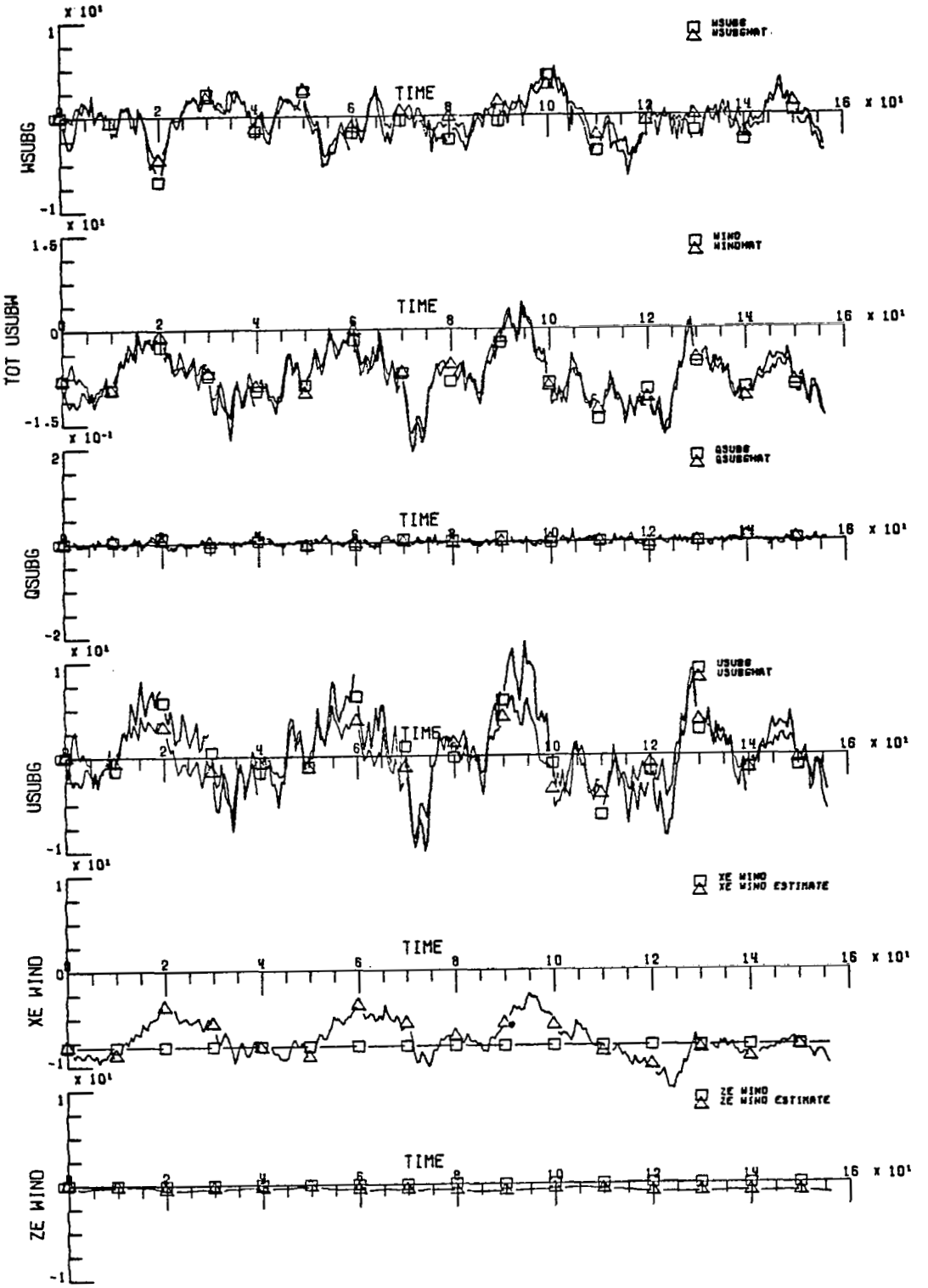

Figure 12C Closed Loop Response Simulation: Meas. Noise Present, High Gusts (τ_u = 4 ft/sec., τ_w = 2 ft/sec.), 8 ft/sec. Tail Wind (1 ft. = 0.3048 m).

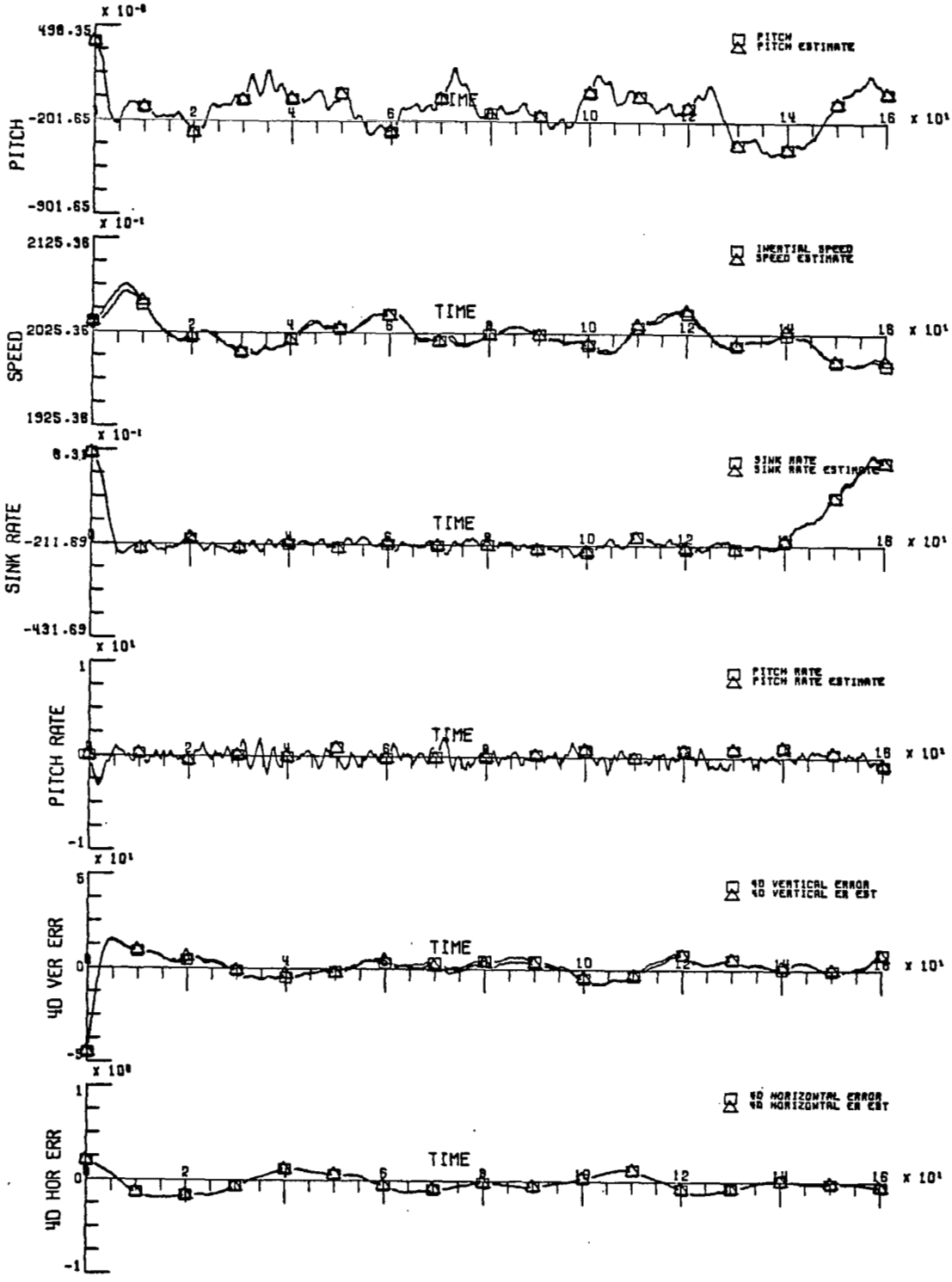

Figure 13A Closed Loop Response Simulation: Meas. Noise Present, High Gusts (τ_u = 4 ft/sec., τ_w = 2 ft/sec.), Wind Shear of 8 ft/sec. per 100 ft. (1 ft. = 0.3048 m).

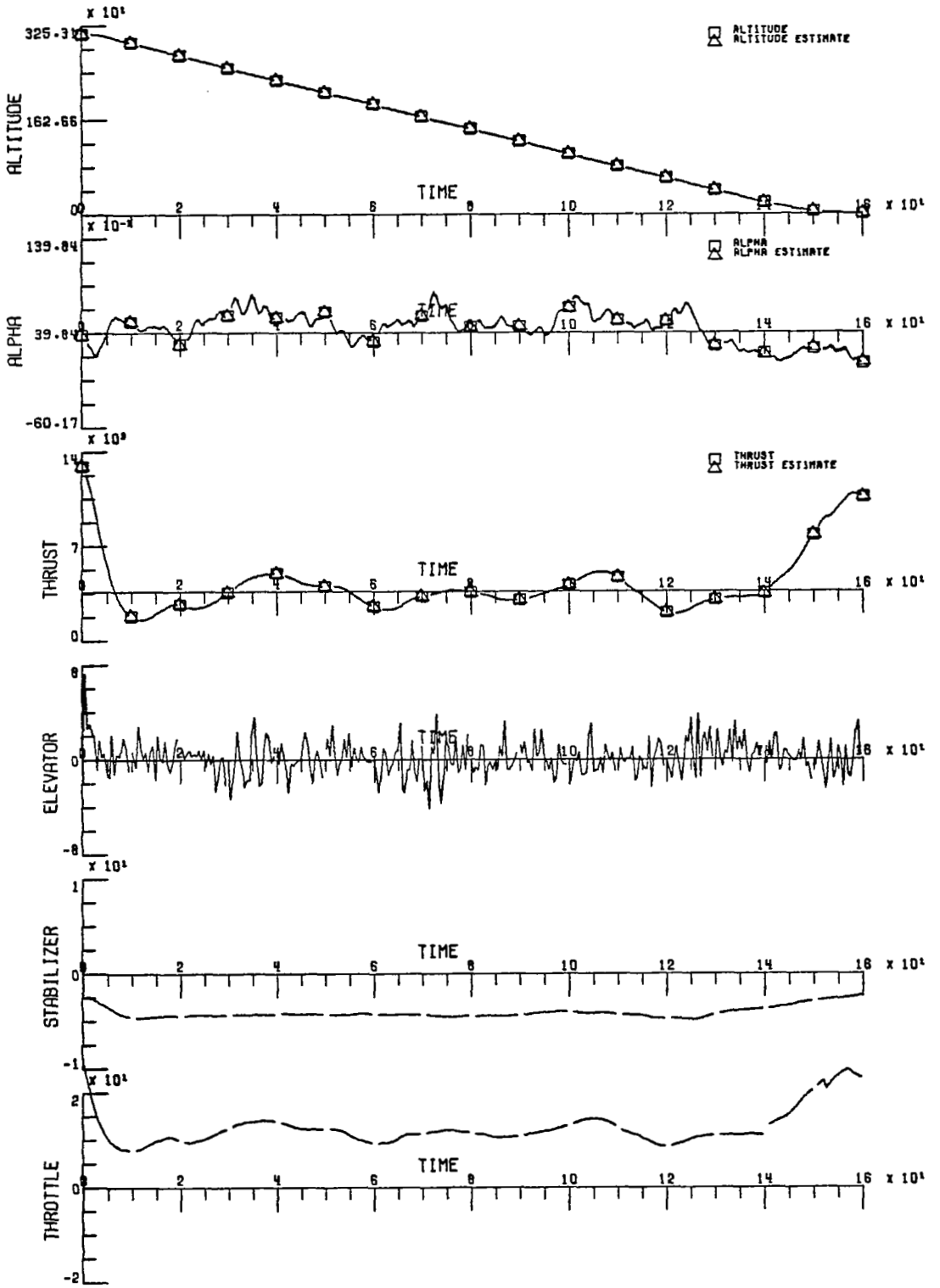

Figure 13B Closed Loop Response Simulation: Meas. Noise Present, High Gusts (τ_u = 4 ft/sec., τ_w = 2 ft/sec.), Wind Shear of 8 ft/sec. per 100 ft. (1 ft. = 0.3048 m; 1 lb. = 4.448 N).

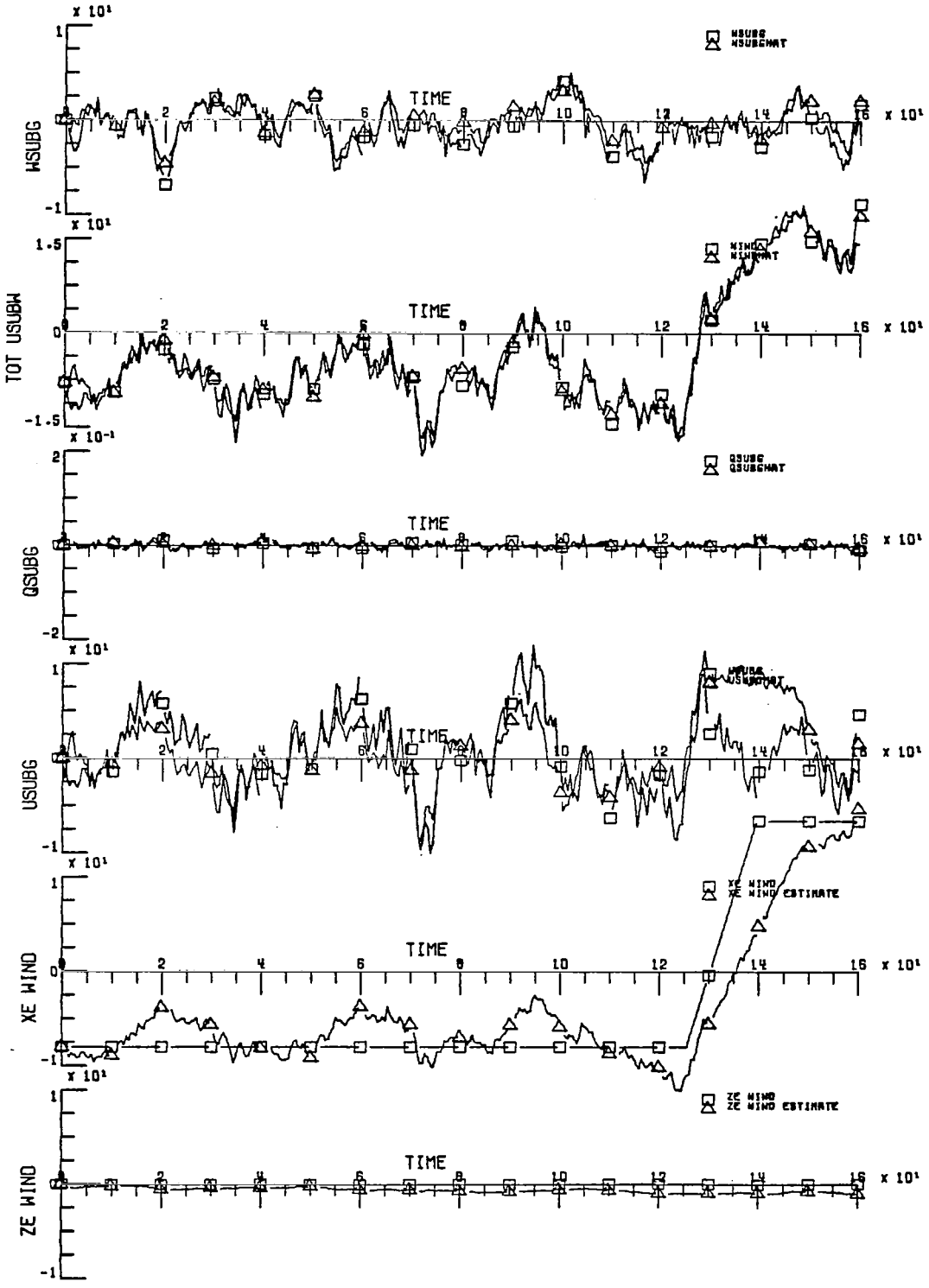

Figure 13C Closed Loop Response Simulation: Meas. Noise Present, High Gusts (τ_u = 4 ft/sec., τ_w = 2 ft/sec.), Wind Shear of 8 ft/sec. per 100 ft. (1 ft. = 0.3048 m).

Table 1 Standard Deviation Values for the Simulation of Sensor Noises

Variable	Standard Deviation	Type
Y_1	.15°	additive
Y_2	.10°/sec	additive
Y_3	1 ft.	additive
Y_4	.031°	additive
Y_5	25 ft.	additive
Y_6	5 %	multiplicative
Y_7	.005 g	additive
Y_8	2 %	multiplicative
Y_9	.005 g	additive

1 ft. = 0.3048 m.

Table 2 Touchdown Conditions

Fig. No. and Wind Conditions	Touchdown pt. (ft.)	Sink Rate (ft/sec.)	Ground Speed (ft/sec.)
7 No meas, Noise, No Winds	1646	1.93	199.2
8 No Winds	1569	2.63	199.2
9 Tail Wind Average Gust	1503	2.28	199.3
10 Wind Shear Average Gust	1607	1.27	199.2
11 Wind Shear Average Gust (MLS Dropout on Glideslope	1607	1.27	199.2
12 Tail Wind High Gust	1480	2.83	199.5
13 Wind Shear High Gust	2284	1.60	199.2

1 ft. = 0.3048 m.

REFERENCES

1. Anon., "A New Guidance System for Approach and Landing," Vol. 2, Radio Technical Commission for Aeronautics, 1717 H Street, N. W., Washington, D. C., Document DO-148, Dec. 18, 1970.

2. Del Balyo, Joseph M. and Stanley R. Jones, United States Program to ICAO for a New Non-Visual Approach and Landing System. AGARD CP-188, Plans and Development for Air Traffic Systems, May 23, 1975.

3. Reeder, J. P., R. T. Taylor and T. M. Walsh, "New Designs and Operating Techniques for Improved Terminal Area Compatibility," SAE, Air Transportation Meeting, Dallas, Texas, April 30, 1974.

4. Roskam, J., "Flight Dynamics of Rigid and Elastic Airplanes," Roskam Aviation and Engineering Corp., 519 Boulder, Lawrence, Kansas, 1972.

5. Halyo, N., "Development of an Optimal Automatic Control Law and Filter Algorithm for Steep Glideslope Capture and Glideslope Tracking," NASA CR-2720, 1976.

6. Chalk, C. R., T. P. Neal, T. M. Harris and E. F. Prichard, "Background Information and User Guide for MIL-F-8785B(ASG), 'Military Specification-Flying Qualities of Piloted Airplanes,'" Air Force Flight Dynamics Report AFFDL-TR-69-72, August 1969.

7. Bode, H. W. and C. E. Shannon, "A Simplified Deviation of Linear Least-Squares Smoothing and Prediction Theory," Proc. IRE, Vol. 38, pp. 417-425, April 1950.

8. Halyo, N. and G. A. McAlpine, "On the Spectral Factorization of Non-Stationary Vector Random Processes," IEEE Trans. on Automatic Control, Vol. AC-19, No. 6, Dec. 1974.

9. Halyo, N. and R. E. Foulkes, "On the Quadratic Sampled-Data Regulator with Unstable Random Disturbances," IEEE SMC Soc. Proc. 1974 International Conf. on Syst., Man and Cybern. pp. 93-103, Oct. 1974.

10. Halyo, N. and A. K. Caglayan, "A Separation Theory for the Stochastic Sampled-Data LQG Problem," International J. of Control, Vol. 23, No. 2, pp. 237-244, Feb. 1976.

11. Kirk, D. E., Optimal Control Theory: An Introduction, Prentice Hall, Inc., Englewood Cliffs, New Jersey, 1970.

12. Hoffman, W. C., W. M. Hollister and R. W. Simpson, "Functional Error Analysis and Modeling for ATC System Concepts Evaluation," DOT, TSC-212-72-1, May 1972.

13. Sorensen, J. A., "Analysis of Instrumentation Error Effects on the Identification of Aircraft Parameters, NASA CR-112121, 1972.

APPENDIX

The aircraft equations of motion which are used in the simulation and for the development of the filter and control law were developed in Section II. The final form of the continuous equations as given in equation (6c) is repeated here for convenience.

$$\dot{x} = Ax + Bu + Dw$$

The form of the matrices A, B and D are also given in Section II. In this appendix, we shall give the expressions for the non-zero elements of these matrices in terms of the aircraft stability derivatives, the stability derivatives are assumed to be in the stability axis.

$$\alpha_1 = -\frac{mg \cos \Theta_o}{\bar{q}_o S}, \qquad \alpha_2 = -\frac{mg \sin \Theta_o}{\bar{q}_o S}$$

$$\alpha_3 = \frac{mU_o}{\bar{q}_o S}, \qquad \alpha_4 = 1/(\alpha_3 + C_{L\dot{\alpha}}),$$

$$\alpha_5 = I_{yy}/\bar{q}_o S\bar{c}, \qquad \bar{q}_o = \frac{1}{2} \rho U_o^2,$$

where S is the wing area, $\bar{c}$ the mean aerodynamics chord and ρ is the air density. Using these variables, the matrix elements are given below.

$$a_{14} = 1$$

$$a_{21} = \frac{\alpha_1}{\alpha_3}, \quad a_{22} = \frac{1}{\alpha_3}(-C_{Du} - 2C_{Do} + C_{Txu} + 2C_{Tx_o}),$$

$$a_{23} = \frac{-C_{D\alpha} + C_{Lo}}{\alpha_3}, \quad a_{27} = \frac{C_{Tx}}{\alpha_3}, \quad a_{28} = -\frac{C_{D\delta s}}{\alpha_3},$$

$$a_{31} = \alpha_2\alpha_4 \ , \ a_{32} = -\alpha_4 \ (C_{Lu} + 2C_{Lo}) \ , \ a_{33} = -\alpha_4 \ (C_{L\alpha} + C_{Do}) \ ,$$

$$a_{34} = \alpha_4 \ (\alpha_3 - C_{Lq}) \quad , \quad a_{37} = \alpha_4 \ C_{Tz}, \ a_{39} = -\alpha_4 \ C_{L\delta s}$$

$$a_{41} = \alpha_4 \ C_{m\dot{\alpha}} \ \alpha_2/\alpha_5 \quad , \quad a_{42} = \frac{1}{\alpha_5} \ (C_{mu} + 2 \ C_{mo} + C_{m\dot{\alpha}} \ a_{32}),$$

$$a_{43} = \frac{1}{\alpha_5} \ (C_{m\alpha} + C_{mT\alpha} + C_{m\dot{\alpha}} \ a_{33}) \ , \ a_{44} = \frac{1}{\alpha_5} \ (C_{mq} + C_{m\dot{\alpha}} \ a_{34}) \ ,$$

$$a_{47} = \frac{C_{mT} + C_{m\dot{\alpha}} \ a_{37}}{\alpha_5} \quad , \quad a_{49} = \frac{C_{m\delta s} + C_{m\dot{\alpha}} \ a_{49}}{\alpha_5}$$

$$a_{77} = -.5 \qquad , \quad a_{78} = .298;$$

$$b_{21} = -\frac{C_{D\delta e}}{\alpha_3} \quad , \quad b_{31} = -\alpha_4 \ C_{L\delta e} \quad , \quad b_{41} = \frac{C_{m\delta e} + C_{m\dot{\alpha}} \ b_{31}}{\alpha_5} \quad ;$$

$$d_{33} = \alpha_4 \ (C_{L\dot{\alpha}} - C_{Lq}) \quad , \quad d_{43} = \frac{C_{mq} + (d_{33} - 1) \ C_{m\dot{\alpha}}}{\alpha_5}$$

Thus, given the stability derivatives of the aircraft, the A, B and D matrices can be computed.